2011

SENSING CHARACTERISTICS OF MULTIWALLED CARBON NANOTUBE (MWCNT) SENSORS EMBEDDED IN POROUS ALUMINA MEMBRANES

Swetha Sree Nimmagadda
University of Kentucky, ssni222@uky.edu

STUDENT AGREEMENT:

I represent that my thesis or dissertation and abstract are my original work. Proper attribution has been given to all outside sources. I understand that I am solely responsible for obtaining any needed copyright permissions. I have obtained and attached hereto needed written permission statements(s) from the owner(s) of each third-party copyrighted matter to be included in my work, allowing electronic distribution (if such use is not permitted by the fair use doctrine).

I hereby grant to The University of Kentucky and its agents the non-exclusive license to archive and make accessible my work in whole or in part in all forms of media, now or hereafter known. I agree that the document mentioned above may be made available immediately for worldwide access unless a preapproved embargo applies.

I retain all other ownership rights to the copyright of my work. I also retain the right to use in future works (such as articles or books) all or part of my work. I understand that I am free to register the copyright to my work.

REVIEW, APPROVAL AND ACCEPTANCE

The document mentioned above has been reviewed and accepted by the student's advisor, on behalf of the advisory committee, and by the Director of Graduate Studies (DGS), on behalf of the program; we verify that this is the final, approved version of the student's dissertation including all changes required by the advisory committee. The undersigned agree to abide by the statements above.

Swetha Sree Nimmagadda, Student

Dr. Vijay Singh, Major Professor

Dr. Zhi Chen, Director of Graduate Studies

SENSING CHARACTERISTICS OF MULTIWALLED CARBON NANOTUBE (MWCNT) SENSORS EMBEDDED IN POROUS ALUMINA MEMBRANES

THESIS

A thesis submitted in partial fulfillment of the
requirements for the degree of Master of Science in the
College of Engineering
at the University of Kentucky

By
Swetha Sree Nimmagadda
Lexington, Kentucky
Director: Dr. Vijay Singh Professor of Electrical Engineering
Lexington, Kentucky
2011

ABSTRACT OF THESIS

SENSING CHARACTERISTICS OF MULTIWALLED CARBON NANOTUBE (MWCNT) SENSORS EMBEDDED IN POROUS ALUMINA MEMBRANES

A theoretical model is developed for calculating the sensitivity of resistive sensors based on aligned multiwall carbon nanotubes (MWCNT) embedded in the pores of alumina membranes. Aligned MWCNTs offer more surface area as each CNT acts as a landing site for detecting gas species. The MWCNTs behave as a p-type semiconducting layer; when the bus bar contacts are placed at either end of the top surface the resistance between the contacts responds to oxidizing (resistance decreases) and reducing gases (resistance increases). The model presented in this thesis aims to understand the device resistance dependence upon the MWCNT resistance, and the sensitivity dependence upon the device structure and design. The model was utilized for enhancing the sensitivity of MWCNT sensors for ammonia (30% sensitivity) and nitrogen dioxide (40% sensitivity) gases. Experimental results from sensitivity measurements are compared with theoretical predictions.

KEYWORDS: Carbon nanotube, resistive sensor, gas sensor, ammonia, semiconductor

Swetha Sree Nimmagadda

14 September, 2011

SENSING CHARACTERISTICS OF MULTIWALLED CARBON NANOTUBE (MWCNT) SENSORS EMBEDDED IN POROUS ALUMINA MEMBRANES

By

Swetha Sree Nimmagadda

Director of Thesis:
Dr .Vijay Singh

Director of Graduate Studies
Dr. Zhi Chen

14 September, 2011

RULES FOR THE USE OF THESES

Unpublished theses submitted for the Master's degree and deposited in the University of Kentucky Library are as a rule open for inspection, but are to be used only with due regard to the rights of the authors. Bibliographical references may be noted, but quotations or summaries of parts may be published only with the permission of the author, and with the usual scholarly acknowledgments.

Extensive copying or publication of the thesis in whole or in part also requires the consent of the Dean of the Graduate School of the University of Kentucky.

A library that borrows this thesis for use by its patrons is expected to secure the signature of each user.

Name	Date

THESIS

Swetha Sree Nimmagadda

The Graduate School

University of Kentucky

2011

Acknowledgments

This work, would not have taken its present shape without the help of several people.

I would like to thank my advisor, Dr. Vijay Singh for giving me the and motivation to work with the theoretical modeling and developing a simulation model of the CNT based resistive sensor.

I would also like to thank Dr. Suresh Rajaputra for his excellent support and ideas all through my work. His excellent ideas, guidance and help were of great help to me. I would sincerely thank him a lot for his patience and time, he put into helping me in my thesis.

I thank Dr. Vijay Singh, Dr. Adams, and Dr. Donohue for their time serving on my committee and for serving their time to read my thesis.

I would also like to thank my fellow group members who allowed me to learn from their work and formulate new ideas, especially Raghu Mangu for his support, ideas and help. I am grateful to him for taking time in helping me with the fabrication of resistive sensor devices. I would also like to thank my friend Venkatesh Gutta for his help in every step and for his encouragement every day of my work.

Finally, without the endless support and blessings from my family members I would not have the courage to stand here through all difficult times. I would like to thank my father, mother and sister for having confidence in me.

Contents

List of Figures

List of Tables

List of Equations

Chapter 1 Introduction

1.1 Introduction

Carbon nanotubes (CNTs) are quasi-one-dimensional nanostructures that exhibit very attractive structural, electrical, optical, and mechanical properties for emerging nanotechnology devices [1]. Some of their inherent properties such as extremely small size, high surface area, high structural and chemical stability and wide spectrum of electrical properties, make them potential gas sensors with improved performance than the conventional solid-state sensors [2].

However, gas sensors based on pristine CNTs have certain limitations, such as sometimes low sensitivity to analytes for which they have low adsorption energy or low affinity, lack of selectivity, or irreversibility or long recovery time. To overcome these limitations, several research groups are currently working on the functionalization of CNTs with different materials to alter their chemical nature and enhance their sensing performance [3].

The electrical properties of multi-walled carbon nanotubes (MWCNTs) are extremely sensitive to charge transfer and chemical doping effects by various molecules. When electron-withdrawing molecules (e.g. NO_2, O_2) or electron-donating molecules (e.g. NH_3) interact with the p-type semiconducting MWCNTs, they will change the density of the main charge carriers (i.e. holes) in the 'bulk' of the nanotube, which changes the conductance of CNTs. As a consequence, electrons are transferred from NH_3 molecule to MWCNTs, decreasing the density of holes, thus increasing the electrical resistance,

shifting the Fermi level away from the valence band. In contrast, electrons are transferred to NO_2 molecule from the valence band of the MWCNTs, increasing the density of holes, thereby decreasing the electrical resistance, shifting the Fermi level towards the valence band. This behavior forms the basis for applications of MWCNTs as electrical chemical gas sensors.

The main objective of this study is to develop a resistive gas sensor structure for mass production with an array of carbon nanotube synthesized on an anodic aluminum oxide (AAO) template, hence we used MWCNTs grown in AAO template. This template was about 60μm thick and pores are of about 40 nm in diameter. For the set of anodization conditions chosen, all the AAO templates had uniform pore diameter and length. Chemical Vapor Deposition (CVD) process was used to grow the CNTs inside the AAO template. The CNTs that grow along the walls of the nano pores take a similar structure thus forming regular arrays of nanotubes of uniform diameter and length. The CNTs grown this way prove to be better gas sensors because of their stable vertical structure. They have better response and recovery times. The grown MWCNT in the template had a wall thickness of 10 nm and were open at both ends. Bus bars were placed along the sensor to measure the resistance across them. When bus bar contacts were placed at both the ends of the top surface, the resistance between these contacts changed accordingly to oxidizing (resistance decreases) and reducing agents (resistance increases).

The deposition creates carbon nano tubes within the pores of the membrane as well as a thin carbon film on the top and bottom sides of the membrane. The thin carbon layer

called the amorphous carbon layer (a-C layer) plays a vital role in determining device baseline resistance and its sensitivity. Electrical contact between tubes was provided by top and bottom conducting layers. The thickness of the a-C layer is inversely proportional to the baseline resistance of the device and its sensitivity. The thickness of the a-C layer can be tailored by changing the conditions in CVD process or by post growth processes. The post growth processes include etching off the a-C layer smoothly by Microwave induced plasma etch, Plasma enhanced chemical vapor deposition etch (PECVD) or Water plasma etch. However in our work we chose Microwave induced plasma etch as it is relatively very simple process.

By using microwave plasma etch technique the top and bottom a-C layer is etched off in steps to study the change in the current path through the device with each etch. The experimental values clearly show the increase in device sensitivity with the etching. The results discussed in this thesis show that the sensor has high sensitivity of around 30.21 % to 100ppm ammonia and 46.32% to 100ppm nitrogen dioxide after plasma etching the amorphous carbon layer by microwave plasma oxidation techniques.

A resistive sensor model was also developed in our work. The primary objective of the resistive sensor model was to understand the device resistance dependence upon the MWCNT resistance and the thickness of amorphous carbon, and the sensitivity dependence upon the device structure and design. With this understanding, the model offered avenues for device improvement.

Etching of the a-C layer completely results in the open circuit of the device where there is no conducting path between the CNTs. So when a metal of higher work function than the CNTs is sputtered over the device, it forms a conducting path over the device. When the metal is sputtered on the top side of the device, the current flows through the metal layer between the electrodes without involving any of the CNTs, hence the sensitivity of the device decreases. However when the bottom side of the device is also sputtered with a metal layer, the metal layer increases the current flowing through the CNTs and hence the sensitivity increases. The present study provides experimental values proving this fact. We chose 3 metals in our work: Gold, copper and nickel. The work functions of theses 3 metals are 5.1eV, 5.04eV and 4.53eV respectively which are higher than that of the CNT (4.2eV). It is known that metals of higher work function than the semiconductor form ohmic contact at the junction and those with lesser work function than the semiconductor form a schottky contact at the junction. Hence the metals we chose form ohmic contact with the CNTs. When metals are deposited over the CNTs they either form a metal layer or nanoclusters, either way they increase the conductivity of the device by forming defect sites for gas adsorption. Due to this additional gas adsorption the sensitivity of the device would be more than that of the pristine CNTs. In our work, when metal was sputtered on both sides of the device the device sensitivity went to as high as 34.2% when exposed to 100ppm ammonia. All the results are discussed further in Chapter 4.

1.2 Objectives and Contributions

The following is the list of objectives and contributions of this thesis:

- The change in device sensitivity and resistance with respect to a-C layer thickness was extensively studied. The higher the thickness of amorphous carbon, the lower the sensitivity.
- Theoretical modeling of the sensor design was proposed and the device resistance was calculated and compared with the actual resistance value.
- Another model was also developed to study the transient response of the device to ammonia gas and nitrogen dioxide gas molecules.
- A program was designed in MATLAB to calculate the resistance of the device.
- Plasma etching technique like plasma oxidation in microwave was performed in order to remove amorphous carbon to improve the sensitivities.
- After the removal of a-C layer, the top and bottom layers were sputtered with a more conductive metal layer to understand the relation of current flow paths with the sensitivity.

1.3 Outline of the thesis

Chapter 1 will give a brief introduction to carbon nanotube and its advantages for being used as a sensor and other applications. Chapter 2 will give a detailed description of the theoretical model of the resistive sensor. A detailed MATLAB program to calculate the device resistance is composed. Theoretical model with the simulation results are all discussed in Chapter 2 and a model for the sensor response to the ammonia molecules and how it changes with respect to sensitivity and the number of electrons donated by test

gas molecules and the acceptor density. Chapter 3 will explain about all the experimental procedures used to prepare the resistive sensor model. Section 3.1 will describe about the anodization of the template and then MWCNTs grown in the template by Chemical Vapor Deposition (CVD) will be discussed in detail in section 3.2. The basic sensor systems used in sensing of the gas analytes and the process of removal of amorphous carbon to improve the sensitivity by microwave plasma oxidation are discussed in sections 3.3, 3.4 and 3.5 respectively. Chapter 4 will discuss the results obtained by microwave plasma oxidation, results obtained by replacing a-C layer with a metal layer and the comparison of the sensor response with three different metals sputtered on the device. Chapter 5 will give the conclusion of the thesis work and provide directions for the future work.

Chapter 2: Theoretical Model

2.1 Description and operating principle of the device model

Anodic Aluminum Oxide (AAO) template was prepared by a two-step anodization method. CVD method was used to grow MWCNTs in the pores of the AAO template. Well-aligned carbon nanotubes were obtained perpendicular to the substrate. A thin amorphous carbon layer (a-C layer) was formed as a byproduct on the surface of the template during the CVD process which connected all the carbon nanotubes electrically. The thickness of this a-C layer determines the baseline resistance of the device and also its sensitivity of response to different gases. After the CVD process the templates are annealed. In order to measure the electrical properties such as resistance, electrical contacts are made on the template by depositing colloidal graphite paste first and then silver paste was deposited over it. The cross sectional view of the device model is shown in Figure 2.1 [4].

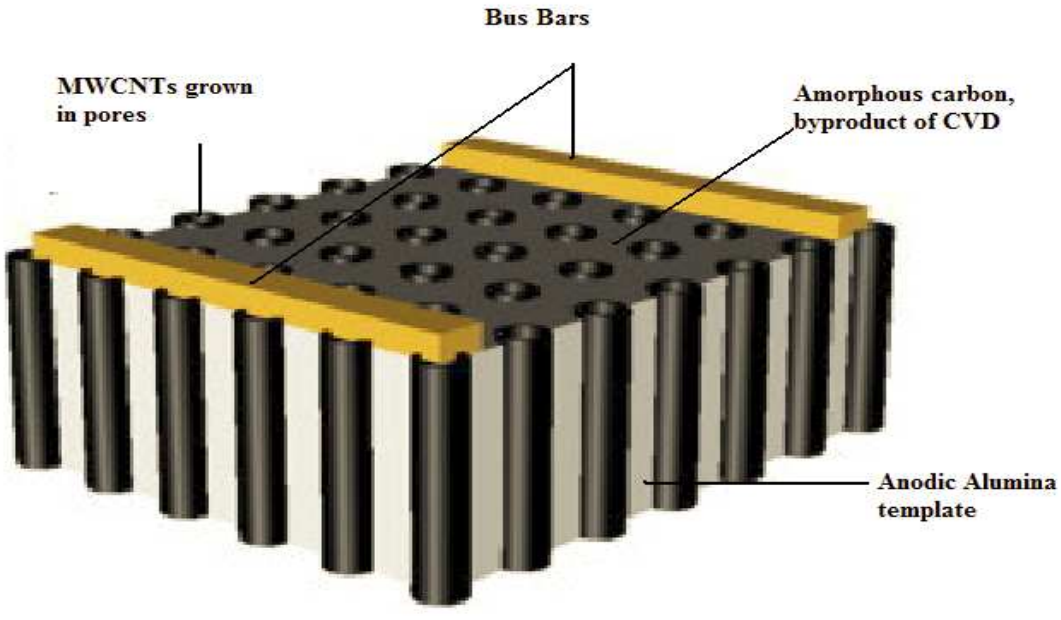

Figure 2.1: Resistance sensor model [4]

The fabricated MWCNT gas sensors exhibit a p-type semiconducting nature with holes as the majority charge carriers. Their electrical properties are extremely sensitive to charge transfer and chemical doping effects by various molecules. When gas molecules interact with the p-type semiconducting CNTs, they will change the majority charge carrier (i.e. holes) concentration in the bulk of the nanotube, which changes the conductance of the CNTs. [5]

When electron withdrawing molecules (like NO_2, O_2) interact with the CNTs, they accept electrons from the CNTs and as a result the hole concentration i.e. the majority carrier concentration increases in the bulk of the CNTs which increases its conductivity. When electron donating molecules (like NH_3) interact with the CNTs, they donate electrons to the CNT which recombine with the holes to decrease the majority carrier concentration and decrease the conductivity.

The sensitivity of response to the gas molecules seems to be related to the amount of charge transfer and the binding energy. The amount of charge transfer in NO_2 molecule is twice that in NH_3 molecule. It is calculated the amount of charge transfer in NO_2 is 0.1e and in NH_3 molecule is 0.04e. [6]

As shown in Figure 2.2 the device can have two current paths [4]

- Direct current path where the current flows through the a-C layer without involving any of the CNTs.
- Alternate current path where the current flows through the CNTs and bottom conducting a-C layer.

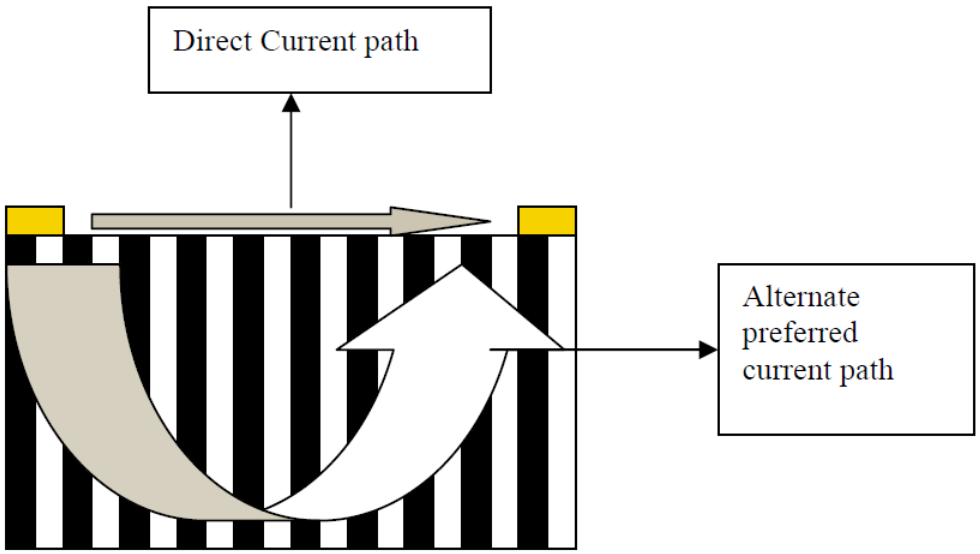

Figure 2.2: Two possible current paths in the resistive sensor model [4]

Since the direct current path does not include any of the CNTs, it does not contribute to the sensitivity of the device and so the alternate current path is preferred over it. The thickness of the a-C layer on both sides of the template can be tailored in a manner so as to make the current flow through the CNTs and thus increase the sensitivity. However after the a-C layer is completely etched off, it can be replaced with a high work function metal to further increase the sensitivity. It is known that metals exhibit a broad range of electronic, chemical and physical properties that are often highly sensitive to changes in their chemical environment. [8]

The resistive sensor model describes the effect thickness of the a-C layer on the baseline resistance and the sensitivity of the device and through this model we could also analyze ways to improve the sensitivity. We have also designed a model to analyze the steady state and transient response of MWCNTs to ammonia and nitrogen dioxide gases.

2.2 The equivalent circuit model for resistive sensor model

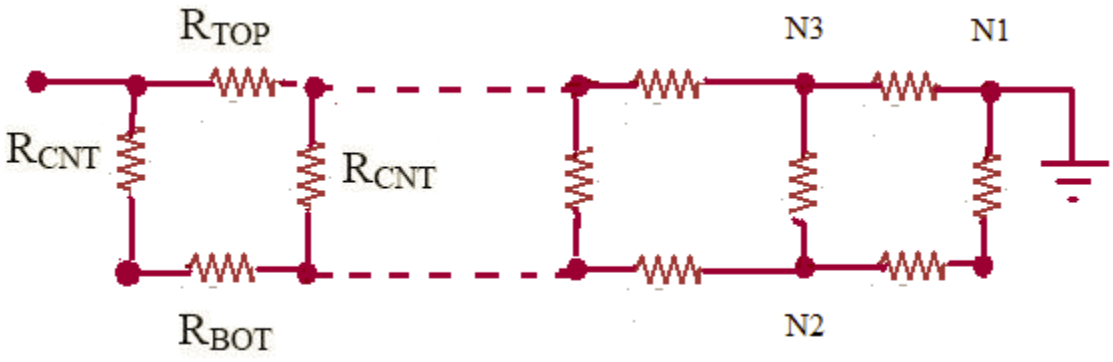

Figure 2.3: Equivalent circuit model showing R_{TOP}, R_{CNT}, and R_{BOT} of one row of 3D regular network of the device. Nodes N1, N2 and N3 are shown as the nodes of the first Δ to Y transformation. [3]

The equivalent circuit model is a regular 3D network of 3 resistances:

- Resistance of the top layer of amorphous carbon (R_{TOP}),
- Resistance of the MWCNT (R_{CNT}), and
- Resistance of the bottom layer of amorphous carbon (R_{BOT}).

This equivalent circuit was developed to understand the operation of the sensor device and to find ways to improve the sensitivity of the device. The equivalent circuit shown in Figure 2.3 is of one row of vertically aligned MWCNT.

2.3 Device of resistance

The equivalent row resistance is calculated by successive Δ-Y transformations along the row.

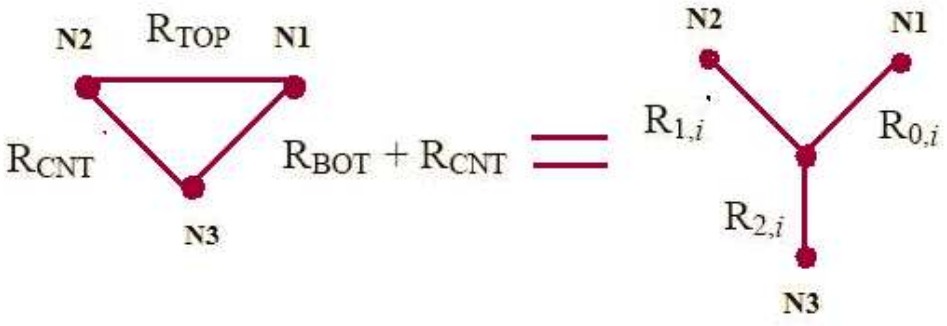

Figure 2.4: The nodes and label for each resistor for the first delta-wye transformation. [3]

The resistance values after the first delta -wye transformation is given by the following equations:

$$R_{0,i} = \frac{R_{TOP}(R_{BOT} + R_{CNT})}{(2R_{CNT} + R_{TOP} + R_{BOT})} \quad (2.1)$$

$$R_{1,i} = \frac{R_{CNT}R_{TOP}}{(2R_{CNT} + R_{TOP} + R_{BOT})} \quad (2.2)$$

$$R_{2,i} = \frac{R_{CNT}(R_{BOT} + R_{CNT})}{2R_{CNT} + R_{TOP} + R_{BOT}} \quad (2.3)$$

After the first transformation, points N1', N2', and N3' are the nodes for second Δ-Y transformation as seen in Figure 2.5.

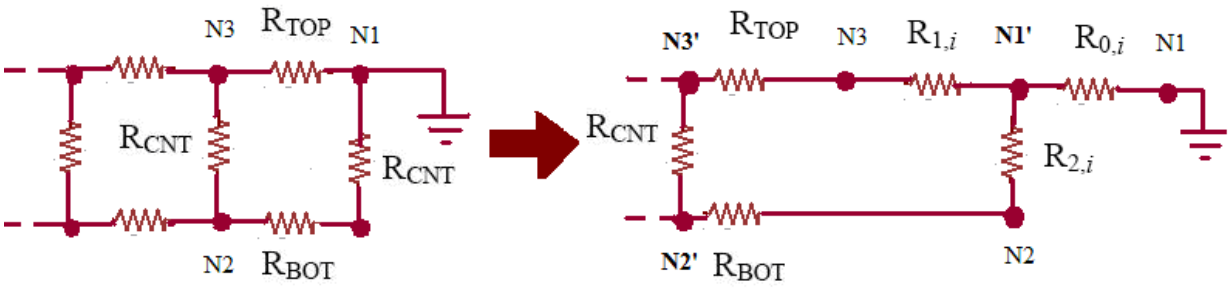

Figure 2.5: Second Delta to Wye transformation

The final equation for equivalent row resistance is shown in Equation 2.4.

$$R_{Row} = \sum_{i=1}^{x} R_{0,i} = \frac{R_{TOP}(R_{BOT}+R_{CNT})}{2R_{CNT}+R_{TOP}+R_{BOT}} + \sum_{i=1}^{x-3} \frac{(R_{TOP}+R_{1,i})(R_{BOT}+R_{2,i})}{R_{CNT}+(R_{TOP}+R_{1,i})+(R_{BOT}+R_{2,i})} + \frac{(R_{TOP}+R_{1,x})(R_{CNT}+R_{BOT}+R_{2,x})}{R_{CNT}+(R_{TOP}+R_{1,i})+(R_{BOT}+R_{2,i})} \quad (2.4)$$

The first term of the equation is $R_{0,1}$ which is the result of first delta to wye transformation. The second term is the summation of all $R_{0,i}$ terms from every transformation and the third term is the parallel resistance of two remaining resistances at the end of the row.

The terms $R_{1,i}$ and $R_{2,i}$ depend on $R_{1,i-1}$ and $R_{2,i-1}$ respectively, as shown in Equation 2.5

$$R_{(1,2),i} = R_{CNT}\frac{R_{(TOP,BOT)}+R_{(1,2),i-1}}{R_{CNT}+R_{(1,i-1)}+R_{(2,i-1)}} \quad (2.5)$$

The device resistance is given by Equation 2.6

$$1/R_{device} = \sum_{i=1}^{y} 1/R_{row} \quad (2.6)$$

where y is the number of rows of MWCNs in y direction.

2.4 Resistance of top and bottom amorphous carbon layers [3]

The resistances of top and bottom layer amorphous carbon layers, R_{TOP} and R_{BOT}, were calculated by using the resistivity formula

$$R = \frac{\rho ac \times L}{A} \tag{2.7}$$

Length L and Area A were calculated taking into consideration that the amorphous carbon does not cover the open pores as shown in Figure 2.6 [3].

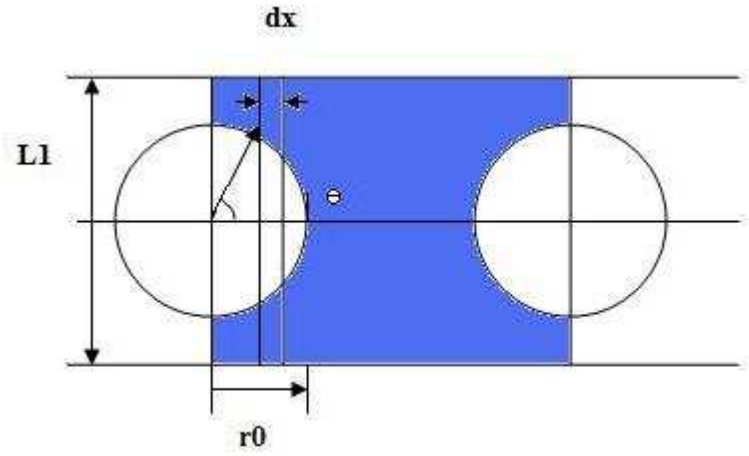

Figure 2.6 Figure shows the shaded area as the conducting path layer of amorphous carbon between adjacent MWCNT's.

In the figure, L1 is the pore pitch in x and y directions, ro is the pore radius and θ is the angle from the x axis inside the pore used in (2.8).

$$R_{(TOP,BOT)} = 2\left(\left(\frac{\rho ac}{2tac_{TOP,BOT}} \int_{\Theta=0}^{\Theta=\frac{pi}{2}} (ro \sin\Theta d\Theta/(L1/2 - ro\sin\Theta)) + \left(\rho ac \frac{\frac{L1}{2ro}}{tac_{TOP,BOT} x\ L1} \right) \right) \right) \tag{2.8}$$

Substituting these values of L1=85nm and r0=20nm which are the standard values of the samples used in our experiments, [2.8] reduces to

$$R_{(TOP,BOT)} = \frac{\rho ac \times 1.29}{tac_{TOP,BOT}} \quad (2.9)$$

2.5 Resistance of MWCNT [3]

The resistance of the carbon nanotube was calculated [3] by:

$$R_{CNT} = \frac{4\rho_{CNT} \times h_{CNT}}{\Pi x(do^2 - di^2)} \quad (2.10)$$

2.6 Parameters used in the model

Table 2.1: Parameters used in resistive sensor model

Standard sample size	1 cm x 0.8 cm ($0.8cm^2$)
Outer diameter of the CNT, do	40 nm
Inner diameter of the CNT, di	30 nm
Number of CNTs in x-direction, Nx	1.27x10^5 pores
Number of CNTs in y-direction, Ny	0.91x10^5 pores
Length of CNTs'	60 μm
Pore density=No. of pores/Area selected	106.5 pores / μm^2
Area of the ring	π x [(20nm)2- (15nm)2]= 549.5 x10^-18 m^2
Resistance of CNT, Rcnt [3]	85.7x10^3 ohms

The standard size of the sample was calculated by taking the average of the sizes of all samples. The outer pore diameter, inner pore diameter and the length of the CNTs are constant values for all templates prepared under same set of standard anodization conditions. The number of CNTs in x and y direction are calculated from Figure 2.7 by using ImageJ software.

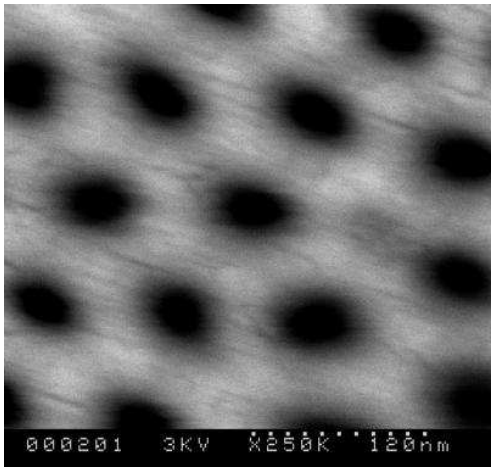

Figure 2.7: Image used to calculate number of pores in x and y direction.

ρ_{CNT} = (R_{CNT} x Area of the ring)/(Length of the CNT)

substituting the values of R_{CNT}, area of the ring and the length of CNT from table 2.1, we get

ρ_{CNT} = 7.8527*10^5 ohm-cm

2.7 Model to analyze steady state and transient response of the device to target molecules

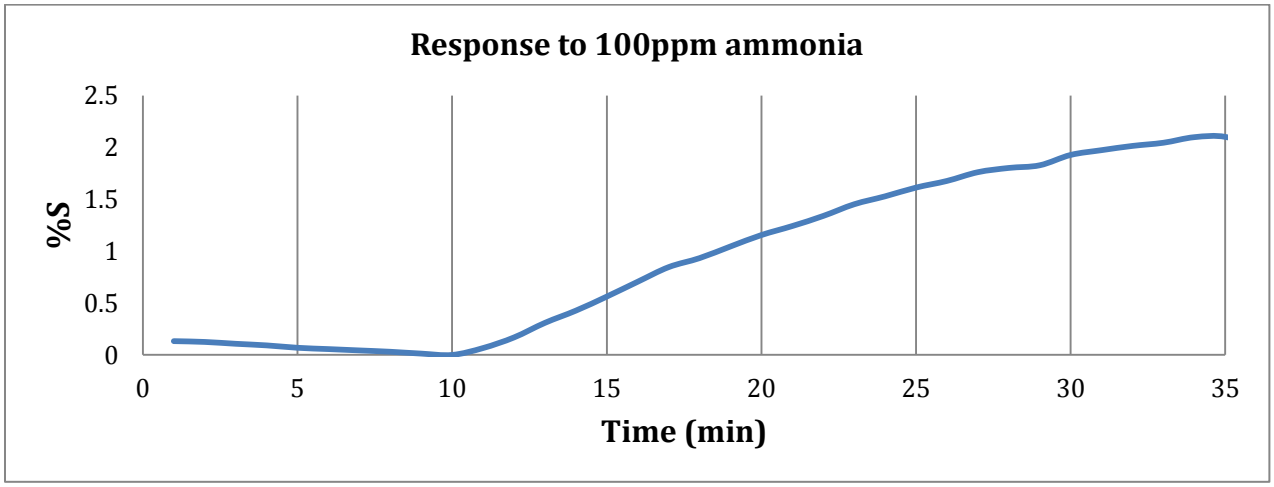

Figure 2.8: Steady state response of MWCNT resistive sensor

Fig 2.8 shows the steady state response of MWCNT resistive sensor. The template is first exposed to N_2 gas until its resistance reaches a constant value. At time t=0 the sample would have a constant resistance, from time t=10 the sample would have transient response where its resistance and sensitivity of the sample increases rapidly when it is exposed to NH_3 gas and decrease rapidly when exposed to NO_2 gas. The test gas (N_2) and target gases (NH_3 and NO_2) were purged into the test chamber at a constant flow rate of 500sccm. The sample slowly reaches a steady state at some time when all the adsorption sites become unavailable. The steady state and transient response of the device is studied mathematically in this section.

2.7.1 Steady state and transient response to ammonia molecules

Flow rate of NH_3 gas into the test chamber=500 sccm

Density of NH_3 gas at room temperature=0.76 g/l

True mass flow=Flow rate in sccm * Gas density at room temp

=500 cc/min *(1/1000) l/cc*0.76g/l

=0.38 g/min

Number of moles of NH_3 gas= $((0.38g/min)/(17.03g/mol))$ =0.0223 mole/min

1 mole contains 6.023*10^23 molecules

0.0223 moles contains 0.0223*6.023*10^23 molecules=0.134*10^23 molecules

1 molecule of NH_3 will donate 0.04 electrons to CNT [2]

0.134*10^23 molecules will accept 0.04*0.134*10^23 electrons

=5.37*10^20 electrons/min

No of excess electrons generated, g=5.37*10^20 electrons/min

T1 is the electron lifetime for the recombination of holes of CNTs and electrons.

The continuity equation is,

$$-\frac{\Delta n(t)}{T1}+g=\frac{d\Delta n(t)}{dt}$$

$$\frac{d\Delta n(t)}{dt}=\frac{gxT1-\Delta n(t)}{T1}$$

Solving the continuity equation we get

$$\Delta n(t)=gT1 + c*\exp(-t/T1) \quad (2.11)$$

At t=0 $\Delta n(t)=0$ => c= -g*T1

c= -5.37*10^20 electrons/min * T1 (2.12)

In steady state $d\Delta n(t)/dt=0$ and $\Delta n=n$

=> n=g*T1

n=5.37*10^20 electrons/min *T1 (2.13)

Before exposure to NH_3 gas

$$\rho cnt= (q*\mu p*po)^{-1} \quad (2.14)$$

where ρ_{cnt}=7.85*10^-5 ohm-cm , q=1.6*10^-19 ,μ_p=10^4 cm^2/Vs

substituting these values we get p_o=0.0796*10^20 cm^{-3}

After exposure to NH_3 gas

$$\rho'_{cnt}=\left(q * \mu p * (po - n)\right)^{-1} \quad (2.15)$$

$$R'_{cnt}=\frac{4* \rho'cnt *hcnt}{\pi*\left(do^2-di^2\right)} \quad (2.16)$$

Assuming

$$\frac{R'_{dev}}{R_{dev}} = \frac{R'_{cnt}}{R_{cnt}} \quad (2.17)$$

$$\frac{11.9692}{11.9323} = \frac{R'_{cnt}}{85.7*10\text{^}4}$$

R'_{cnt}=85.965*10^3 ohm

Substituting (2.15) in (2.16)

$$R'_{cnt} = \frac{4 * hcnt}{\pi * (do^2 - di^2) * q * \mu p * (po - n)} \quad (2.18)$$

Where hcnt=60µm

Do=40nm

Di=30nm

Q=1.6*10^-19 Coulombs

µp=10^4 cm^2/Vs

po=0.0796*10^20 cm^{-3}

g=5.37*10^20 electrons/min

R'_{cnt}=85.965*10^3 ohm

Substituting the above values and (2.13) in (2.18)

We get T1=85.52µs

Substituting above value in (2.12)

c= -5.37*10^20 electrons/min * 85.52*10^-6= -4.592*10^16

Therefore, Δn(t)= 4.592 x10^16x(1-exp(-t/85.52x10^-6) e- per second (2.19)

2.7.2 Steady state and transient response to nitrogen dioxide molecules

Flow rate of NO_2 gas into the test chamber=500 sccm

Density of NO_2 gas at room temperature=3.4 g/l

True mass flow=Flow rate in sccm * Gas density at room temp

=500 cc/min *(1/1000) l/cc*3.4g/l =1.7 g/min

Number of moles of NO_2 gas= ((1.7g/min)/(46.0056g/mol))=0.03695 mole/min

1 mole contains 6.023*10^23 molecules

0.03695 moles contains 0.03695*6.023*10^23 molecules=0.2226*10^23 molecules

1 molecule of NO_2 will accept 0.10 electrons from CNT

0.2226*10^23 molecules will accept 0.10*0.2226*10^23 electrons=0.02226*10^23 electrons/min

No of excess electrons generated, g=0.02226*10^23 electrons/min

T1 is the electron lifetime for the recombination of holes of CNTs and electrons.

Solving the continuity equation we get

$$\Delta n(t)=gT1 + c*\exp(-t/T1) \quad (2.20)$$

At t=0 $\Delta n(t)=0$ => $c=-g*T1$

$$c=-0.02226*10^{23} \text{ electrons/min} * T1 \quad (2.21)$$

In steady state $d\Delta n(t)/dt=0$ and $\Delta n=n$ => $n=g*T1$

$$n=0.02226*10^{23} \text{ electrons/min} *T1 \quad (2.22)$$

Before exposure to NO_2 gas

$$\rho_{cnt=}(q * \mu p * po)^{-1} \quad (2.23)$$

where ρ_{cnt}=7.85*10^-5 ohm-cm , q=1.6*10^-19 ,μ_p=10^4 cm^2/Vs

substituting these values we get p_o=0.0796*10^20 cm^{-3}

After exposure to NO_2 gas

$$\rho'_{cnt}=\left(q * \mu p * (po + n)\right)^{-1} \quad (2.24)$$

$$R'_{cnt}=\frac{4* \rho'cnt *hcnt}{\pi*\left(do^2-di^2\right)} \quad (2.25)$$

Assuming

$$\frac{R'_{dev}}{R_{dev}} = \frac{R'_{cnt}}{R_{cnt}} \quad (2.26)$$

$$\frac{26.888}{36.172} = \frac{R'_{cnt}}{85.7*10^4}$$

R'_{cnt}=63.7*10^3 ohm

Substituting (2.24) in (2.25)

$$R'_{cnt}=\frac{4* hcnt}{\pi*\left(do^2-di^2\right)*q*\mu p*(po+n)} \quad (2.27)$$

Where hcnt=60µm

Do=40nm

Di=30nm

Q=1.6*10^-19 Coulombs

µp=10^4 cm^2/Vs

po=0.0796*10^20 cm^{-3}

g=0.02226*10^23 electrons/min

R'_{cnt}=63.7*10^3 ohm

Substituting the above values and (2.22) in (2.27)

We get T1=28.69µs

Substituting above value in (2.21)

C = -0.02226*10^23 electrons/min * 28.69*10^-6 = -6.387*10^16

Therefore, $\Delta n(t)$= 6.387 x10^16x(1-exp(-t/28.69x10^-6) e- per second (2.28)

Equation (2.19) and (2.28) describe the transient response of MWCNT resistive sensor to ammonia and nitrogen dioxide molecules respectively.

Assumptions in the model are:

- In this model, it was assumed that all the sites available for adsorption. However, there was a deviation in the theoretical and practical values because usually all the sites were not available for adsorption as there were some defects in formation of few CNTs.
- The plasma also etched off the a-C layer from the tips of the nanotube in an anisotropic manner resulting in non-uniform thickness of a-C layer. As a consequence, the calculation of the device resistance assuming that the a-C layer was covering whole of interpore region resulted in the deviation of measured device resistance from calculated device resistance.
- Plasma etching of a-C also affected the tips of the CNTs in different ways and changed the work function in different manners [7-9]. Plasma etching of the top and bottom a- C layers results in the partial/complete removal of the a-C layer and change in the work function of MWCNT [7-9].

2.8 Implementing the resistive sensor model and transient response model to calculate device resistance and sensitivity to ammonia molecules using Matlab

The resistive senor model and transient response model are used to calculate the device baseline resistance and sensitivity of the device. The models are implemented in Matlab and the results are summarized in this section. However there is a deviation in the calculated and the measured values because of the assumptions in the model as mentioned in previous section.

In order to calculate the baseline resistance of the device, it is required to determine the thickness of the top and bottom a-C layer. Usually the thickness of the a-C layer can be measured from the cross sectional view of the device. However, thin a-C layer of less than 10nm cannot be measured from the SEM image. Hence a matlab program is written to estimate the thickness of the top and bottom a-C layers from the actual baseline resistance of the device. The results of the program, i.e the thickness of the top and bottom a-C layers are listed in Table 2.2.

Table 2.2: Thickness of top and bottom a-C layers estimated from the matlab program

Sample name	**Condition of plasma etch**	**Baseline Resistance**	**Ttop(nm)**	**Tbot(nm)**
SSMWCNT01	As prepared	11.93 K ohm	2.595	20
	30sec plasma etch(top)	12.58 K ohm	2.448	20
	30sec plasma etch(bottom)	174.76 K ohm	0.385	0.001
	30sec plasma etch(top)	233.62 K ohm	0.289	0.001
SSMWCNT02A	As prepared	39.12 K ohm	0.6	17.57
	15sec plasma etch(top)	59.77 K ohm	0.299	14.8
	30sec plasma etch(top)	66.61 K ohm	0.241	13.62
	30sec plasma etch(bottom)	125.98 K ohm	0.241	0.328
SSMWCNT02B	As prepared	29.13 K ohm	0.832	21
	15sec plasma etch(top)	30.84 K ohm	0.897	21
	30sec plasma etch(top)	32.76 K ohm	0.767	21
	30sec plasma etch(bottom)	169.05 K ohm	0.398	0.001

Substituiting these values of thicknesses and the value of ρ'_{CNT} from equations (2.15) and (2.16) R_{gas} is calculated and from the values of R_{gas} and measured baseline resistance, sensitivity of the device is calculated. As stated earlier, due to the assumptions of the model there is a difference between the calculated and measured sensitivity of the device.

Table 2.3: Comparison of calculated and measured values of gas resistance

Sample name	**Condition of plasma etch**	**Measured Rgas**	**Calculated Rgas**	**Error**
SSMWCNT01	As prepared	11.97K ohm	12.62 K ohm	0.65
	30sec plasma etch(top)	12.61 K ohm	13.35 K ohm	0.74
	30sec plasma etch(bottom)	185.67 K ohm	184.35 K ohm	1.32
	30sec plasma etch(top)	304.2 K ohm	299.1 K ohm	5.1
SSMWCNT02A	As prepared	39.94 K ohm	43.73 K ohm	3.79
	15sec plasma etch(top)	62.94 K ohm	65.797 K ohm	2.857
	30sec plasma etch(top)	70.36 K ohm	72.56 K ohm	2.2
	30sec plasma etch(bottom)	138.36 K ohm	139.43 K ohm	1.07
SSMWCNT02B	As prepared	32.19 K ohm	34.15 K ohm	1.96
	15sec plasma etch(top)	32.21 K ohm	36.54 K ohm	4.33
	30sec plasma etch(top)	36.4 K ohm	39.28 K ohm	2.88
	30sec plasma etch(bottom)	169.48 K ohm	172.67 K ohm	3.19

Table 2.4: Comparison of measured and calculated sensitivities of the device

Sample name	**Condition**	**Measured %S**	**Calculated %S**	**Error**
SSMWCNT01	As Prepared	0.309	5.78	5.471
	30sec plasma etch(top)	0.305	6.12	5.815
	30sec plasma etch(bottom)	6.24	5.48	0.76
	30sec plasma etch(top)	30.21	28.03	2.18
SSMWCNT02A	As prepared	2.101	5.73	3.629
	15sec plasma etch(top)	5.307	9.16	3.86
	30sec plasma etch(top)	5.98	8.2	2.22
	30sec plasma etch(bottom)	9.84	9.65	0.19
SSMWCNT02B	As prepared	4.37	4.7	0.33
	15sec plasma etch(top)	10.56	15.6	5.04
	30sec plasma etch(top)	11.1	16.6	5.5
	30sec plasma etch(bottom)	11.5	13.09	1.59

2.9 Calculation of I_{top} and I_{bot}

The currents through the top and bottom a-C layers (I_{top} and I_{bot}) were calculated from the simulation model in order to study the change in the current paths with change in thickness of the a-C layers. In order to do this calculation, a total current of 1µA was assumed to flow through the device, this current would divide between the direct and alternate current paths as shown in Figure 2.9.

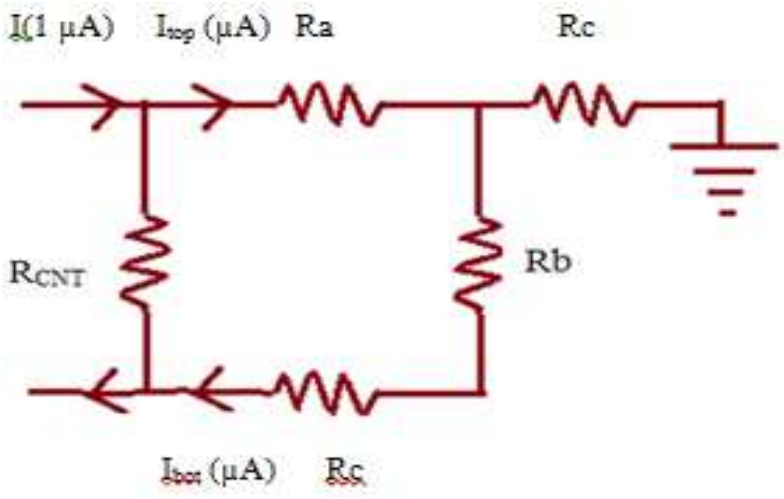

Figure 2.9: Current dividing between direct and alternate current path.

Where, Ra is the sum of all $R_{1,i}$ terms for values of i from 1 to Nx-1, R_b is the sum of all $R_{2,i}$ terms for values of i from 1 to Nx-1 and Rc is the sum of all $R_{0,1}$ terms for values of i from 1 to Nx-1. I_{top} is the current through the direct path (through the top a-C layer) and I_{bot} is the current through the alternate current path (through the CNTs and bottom a-C layer). By using the concept of current divider circuit both the currents are calculated as follows

$$Itop = I^* \frac{R_{CNT}+R_{BOT}+R_b}{R_{TOP}+R_{BOT}+R_{CNT}+Ra+Rb} \quad (2.29)$$

$$Ibot = I^* \frac{Ra}{R_{TOP}+R_{BOT}+R_{CNT}+Ra+Rb} \quad (2.30)$$

Table 2.5 shows the values of I_{top} and I_{bot} for the sample SSMWCNT01. By looking at the current flow the device operation is understood more clearly.

Table 2.5: I_{top} and I_{bot} currents for the sample SSMWCNT01

Condition of plasma etch	Baseline Resistance	T_{top}(nm)	T_{bot}(nm)	I_{top}(μA)	I_{bot}(μA)
As prepared	11.93 K ohm	2.59	20	0.825	0.175
30sec plasma etch(top)	12.58 K ohm	2.45	20	0.817	0.183
30sec plasma etch(bottom)	174.76 K ohm	0.39	0.001	0.997	0.003
60sec plasma etch(top)	233.62 K ohm	0.29	0.001	0.996	0.004

Is is seen that when the device had a-C layers of thickness 2.59nm and 20nm on the top and bottom respectively, currents of 0.825μA and 0.175μA flowed through the top (direct current path) and bottom (alternate current path) current paths. It means that 82.5% of the current flowed through the direct current path while only 17.5% of the current flowed through the alternate current path which involves the CNTs and the bottom a-C layer. By plasma etching the a-C layer on the top and bottom gradually, the current through the alternate path decreased and that through the direct path increased. Finally 99.6% of the current was flowing through the direct current path after 60sec plasma etch on top and 30sec plasma etch on bottom, where the measured sensitivity of the device was 30.21%. This clearly explains the change in the current path with decrease in thickness of the a-C layer. Table 2.6 shows the values of I_{top} an I_{bot} for 2 other samples.

Table 2.6: I_{top} and I_{bot} for samples SSMWCNT02A and SSMWCNT02B

Sample name	Condition of plasma etch	T_{top}(nm)	T_{bot}(nm)	I_{top}(μA)	I_{bot}(μA)
SSMWCNT02A	As prepared	0.6	17.57	0.52	0.48
	15sec plasma etch(top)	0.3	14.8	0.36	0.64
	30sec plasma etch(top)	0.24	13.62	0.3	0.7
	30sec plasma etch(bottom)	0.24	0.33	0.53	0.47
SSMWCNT02B	As prepared	0.9	21	0.62	0.38
	15sec plasma etch(top)	0.83	21	0.6	0.4
	30sec plasma etch(top)	0.77	21	0.58	0.42
	30sec plasma etch(bottom)	0.4	0.001	0.997	0.003

In general the change in currents through top and bottom a-C layers with change in thickness of top a-C layer is given by Figure 2.9. The thickness of top a-C layer (T_{top}) is varied from 0 to 30nm and the thickness of bottom a-C layer is kept constant at 30nm to measure the currents from the sensor model. Clearly from Figure 2.9 as the thickness of top a-C layer increases, I_{top} decreases and I_{bot} increases. Figure 2.10 shows the change in currents with change in T_{bot}.

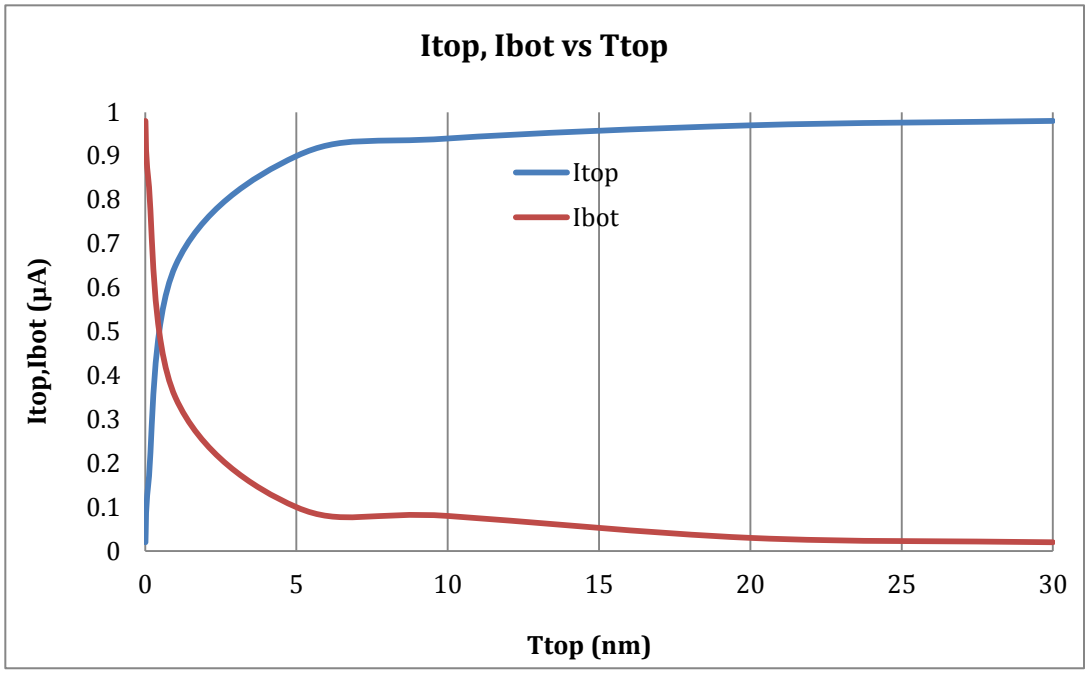

Figure 2.10: I_{top}, I_{bot} vs T_{top}

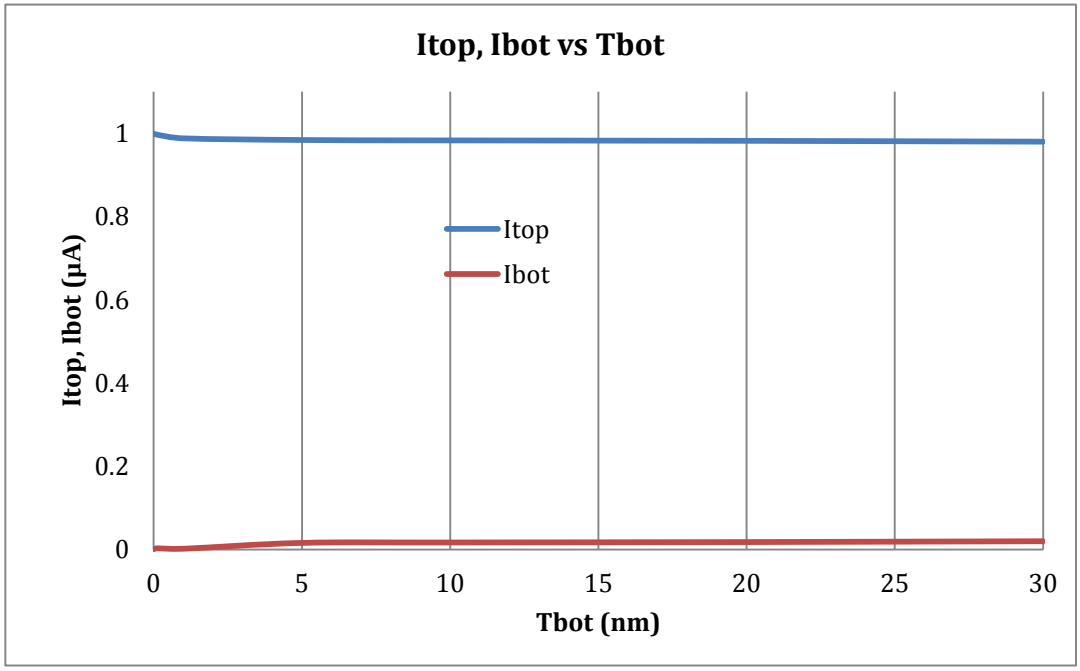

Figure 2.11: I_{top}, I_{bot} vs T_{bot}

Chapter 3: Experimental procedure

3.1 Preparation of AAO template by two-step anodization method

AAO templates were prepared by two-step anodization process. The anodization setup is shown in Figure 3.1. The anodization was conducted in 0.3M oxalic acid with highly pure aluminum tape as anode and a 1 inch square Pt electrode as the cathode.

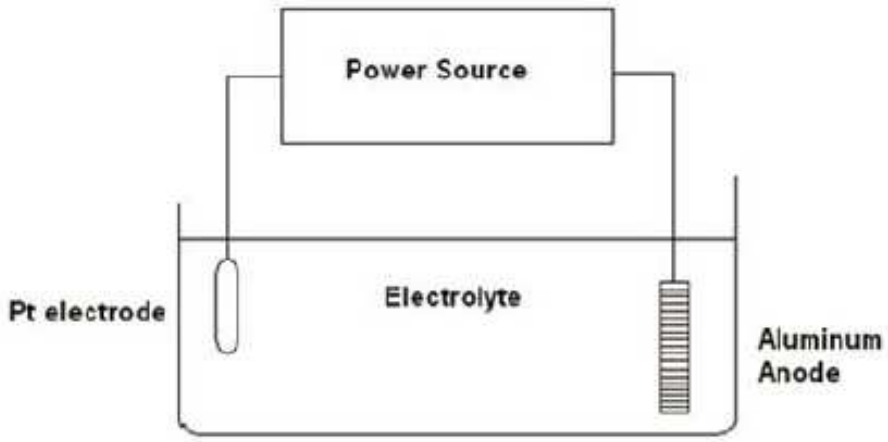

Figure 3.1: Anodization setup

Aluminum tape was cut into 1 inch square size, it was then degreased and cleaned with series of organic solvents and then dried with flowing nitrogen gas. Both the electrodes were placed in a anodization setup, with the voltage and the current supplied using a Kepco (Model ABC 125-1DM) programmable constant DC power supply at a low temperature. The first anodization step was performed for 15mins under constant voltage and current of 30V and 50mA respectively. The anodized template is now heated in a mixture of phosphoric acid (5 wt.%) and chromic acid (10 wt.%) at 85^0C to remove the aluminum oxide layer. However, the pores formed during this anodization step were poor and not uniform and so a second anodization step of longer duration (21-22 hours) was performed. The templates were then soaked in a mixture of cupric chloride and HCl acid

solution for 3hrs so that the aluminum was completely etched off. The templates thus obtained were floated on 5% phosphoric acid for 2mins at 60^0C to remove the barrier layer and widen the pores. Finally, the templates were thoroughly rinsed in de-ionized water and annealed for 2hrs at 750^0C in an oxygen environment [3].

3.2 Growth of MWCNT in the pores of AAO template by CVD process

In this process, pure xylene [$C_8H_{10}(C_6H_4C_2H_6)$] was used as hydrocarbon source in a stream of nitrogen gas. The MWCNTs were grown in CVD system having a 96mm diameter Lindberg furnace, with a specially designed gas flow injector to minimize turbulent flow. The protocol followed for CVD was to first heat the sample to 700^0C where nitrogen was purged at 675 sccm for almost 1 hour. After that, xylene was injected at the rate of 30ml/hr into the preheater having a temperature of 250^0C using a syringe pump for the first 2mins. The rate of Xylene injection was reduced to 1ml/hr for the whole process when xylene vapors were observed to flux out from the outlet of preheater. The xylene vapors were swept by the stream of nitrogen gas swept into the furnace whose temperature was maintained at 700^0C. In this furnace, pyrolysis of xylene takes place to produce carbon nanotubes within the AAO pores without the use of catalyst for 1hour. The sample was then allowed to slowly cool in nitrogen. In this process a-C layer is formed on the top and bottom sides of the template as a byproduct [3].

3.3 Placing the contacts for measurement

MWCNTs were embedded in the pores of AAO templates. Initially graphite paste is placed at both the edges of the sample, after the graphite paste is dry silver paste is applied over it to form the bus bars. These bus bars form the electrical contact to read the resistance change across the sample upon exposure to the test gas.

3.4 Measurement Setup

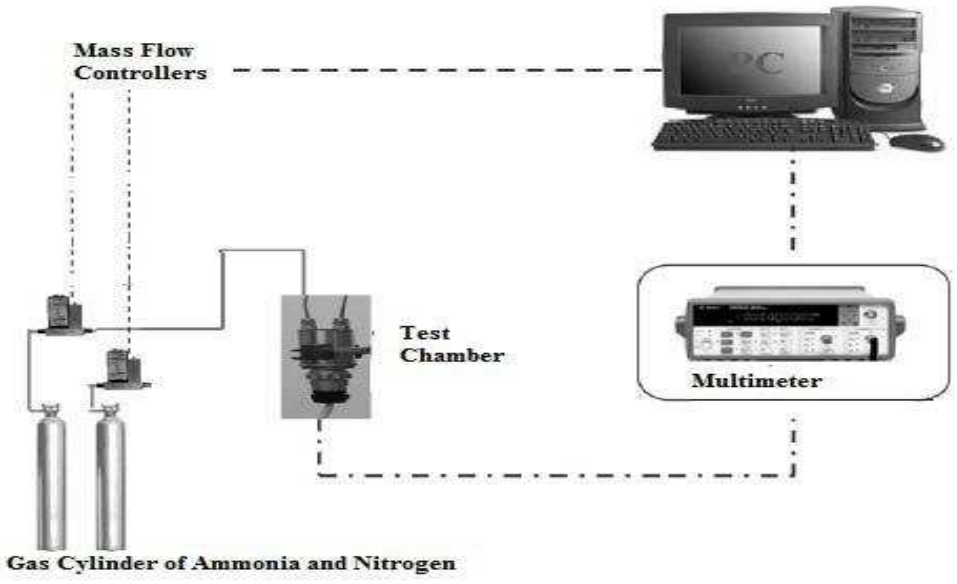

Figure 3.2: Measurement Setup

The measurement setup is shown in Figure 3.1. When the device is ready for measurements it is placed in the test chamber. The test chamber has two electrodes, which are placed on the device bus bars. The electrodes are connected to the HP 3478A digital multimeter. The test chamber is also connected to the target and test gas cylinders through two mass flow controllers. The mass flow controllers maintain a constant flow rate of 500sccm. When the gases are allowed to flow through the test chamber, the resistance change is measured by the multimeter. All the sensitivity measurements were done at room temperature.

The sensitivity of the device is given by

$$\text{Sensitivity } \% = \frac{(\text{Rgas-Rdev})}{\text{Rdev}} * 100$$

where R_{dev} was the device baseline resistance in the presence of carrier gas N_2 and Rgas is the resistance in the presence of the test gas(ammonia or nitrogen dioxide).

3.5 Microwave Induced Plasma Etch of the a-C layer

Microwave plasma oxidation was used for the plasma etching of the amorphous carbon layer. The machine used for microwave plasma etching is a conventional microwave oven which has been modified to allow for a vacuum chamber process gases to run through the back. Oxygen is used to create a plasma inside the glass vacuum chamber, where the sample has been loaded to etch. A power control device has also been added to allow for more precise control of the etching process. In our work etching was done at a constant power level of 75W with varying time intervals as in Tables 4.1 and 4.2.

3.6 Metal sputtering

RF-sputtering system was used to deposit metal layer on the templates after the a-C layer was completely etched off. The sample was placed in the vacuum chamber after venting it fully. The target (here 99.5% pure gold, copper or nickel) was placed on the gun.Inert gas like Ar was purged into the vacuum chamber at a flow rate of 15 sccm. The RF power was tuned to 75 W power. When the plasma was formed, a metal layer of 5nm thickness was sputtered in the inert gas environment. After the deposition of the metal layer of desired thickness on the sample, Ar gas flow was turned off and the vacuum chamber was pumped down. The sample was taken out from the chamber and the target

was removed from the gun. After closing the chamber lid, the pump was turned on again [3]. Since metals of higher work function form a good ohmic contact with p-type semiconducting MWCNTs, we chose Au, Cu and Ni metals to sputter on the top and bottom sides of the template after the removal of a-C layer through microwave plasma etching.

Chapter 4: Results and Discussions

4.1 Effect of a-C layer on the sensitivity of the device.

MWCNTs formed by the CVD process are usually coated with a thin a-C layer (0.1-40 nm) on both sides. This graphite-like a-C layer has a high sp^2 C-C structure. Typically, the a-C film has a very low density (1.2-1.5 g/cm^3), very low bandgap (0-0.6eV), very low sp^3 content (0-30%) and high electrical resistance. [10] The device baseline resistance is inversely proportional to the thickness of the a-C layer.

As described earlier, when the sensor device is exposed to any gas, there are two current paths-direct and alternate current paths. When a device is exposed to NH_3 gas, electrons are donated from the NH_3 gas molecules to the a-C film. This causes a change in the electrical conductance, which results in the current flow across the a-C layer. This current path is considered to be the direct current path. The charge transfer between the NH_3 gas and the CNTs will result in the current through the CNTs. This current path is considered to be the alternate current path. If the device has a thick a-C layer (~30-40nm), there might be very little current through the CNTs and so the sensitivity of the device is very low. However, if we decrease the thickness of the a-C layer, there would be more charge transfer between the gas molecules and the CNTs. Hence the current through the alternate path increases and the sensitivity also increases. The sensitivity would further increase if the thickness of the bottom a-C layer is also reduced.

Conceptually, the device becomes sensitive to gas species when the direct current path becomes too resistive and the current chooses the alternate path. Therefore, the device configuration to get the highest sensitivity to ammonia molecules should be as follows [3]:

- The device should have thinner layer of a-C, such that $R_{Top} > R_{Bot}$, such a device will yield a higher sensitivity than samples with the bus bars on the thick a-C layer ($R_{Top} < R_{Bot}$).
- A modified bottom layer to reduce the resistance of R_{Bot} will yield higher sensitivity**.**
- Removing the a-C layer on the top and bottom sides of the template and replacing it with a higher conductive layer by metal.

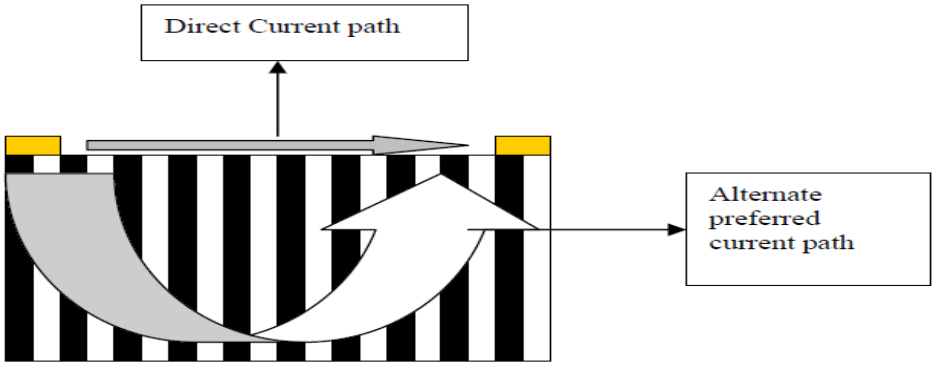

Figure 4.1: Resistive sensor model showing the 2 current flow paths: Direct current path and the alternate preferred path through MWCNTs and bottom conducting amorphous carbon layer

4.2 Effect of Microwave induced plasma etch of the a-C layer on the sensitivity of the device

The thickness of amorphous carbon (a-C) layers can be modified by both post growth processing as well as by tailoring the CVD growth conditions. Post growth processing includes various methods like Microwave Induced Plasma Etch, Plasma Enhanced Chemical Vapor Deposition (PECVD) and Reactive Ion Etching (RIE). However we

chose Microwave Induced Plasma Etch over the others as it is a simpler process. Oxygen was used to create plasma inside a glass vacuum chamber, where a sample has been placed to etch. Etching was done at a constant power level of 75W and at different time intervals to know the effect of the a-C layer on the sensitivity of the device. The sensor devices developed in AAO templates were highly responsive to ammonia and nitrogen dioxide molecules and the lower response time and recovery times were observed. Figure 4.2 shows the thicknesses of the a-C layer before and after microwave plasma etch.

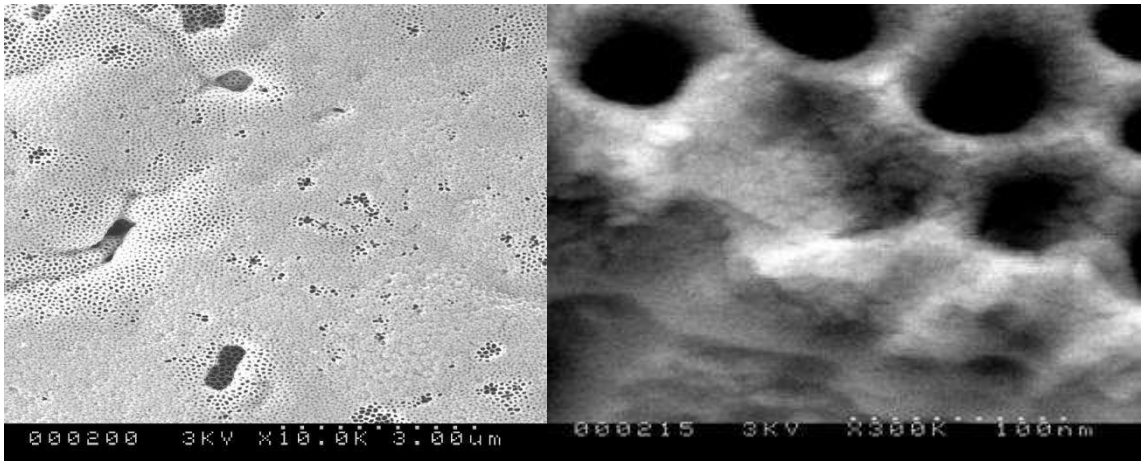

Figure 4.2: Figures showing thickness of a-C layer before and after microwave plasma etch.

4.2.1 Sensor Response of MWCNT resistive sensor

The MWCNT based sensor devices fabricated as discussed in section 3.1.3 were characterized for their sensor response. These sensors were highly responsive to both reducing gases like NH_3 and oxidizing gases like NO_2. The sensor response was evaluated by measuring the resistance upon exposure to various gases. The sensitivity (S) is defined as,

$$\text{Sensitivity } \% = \frac{(R_{gas} - R_{N2})}{R_{N2}} * 100 \qquad (4.1)$$

Where R_{N2} is the device resistance in the presence of carrier gas N_2, and R_{gas} is the resistance in the presence of test gas.

Figures 4.3 a and b show the response of the sample SSMWCNT01A to different microwave induced plasma etch conditions.

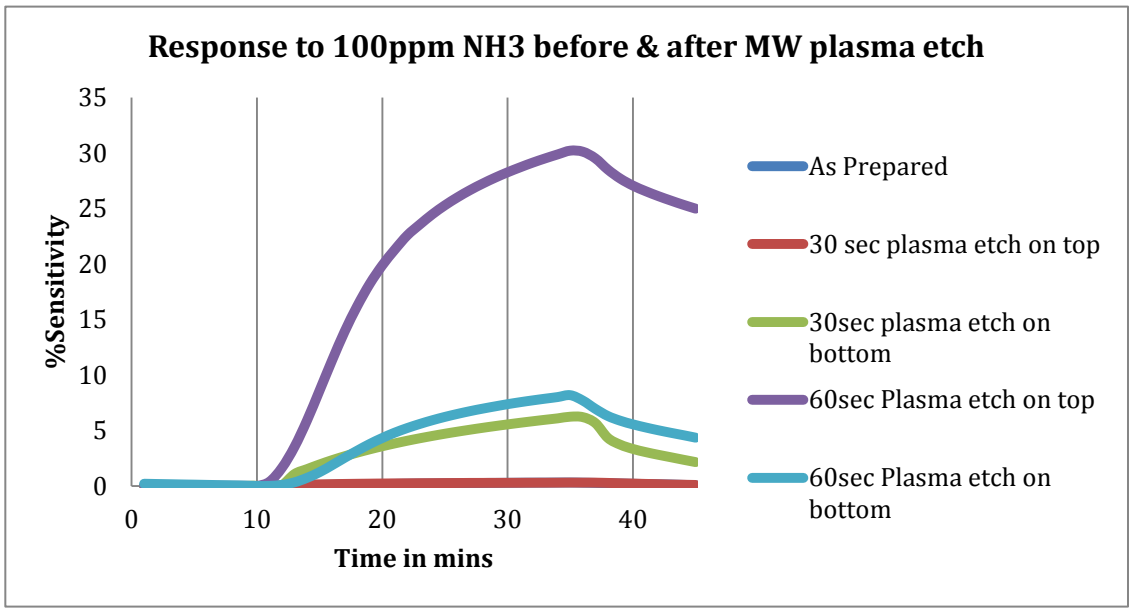

Figure 4.3(a): Steady state response of MWCNT resistive sensor at room temperature at different microwave plasma etch conditions to 100ppm NH_3 gas

These sensor devices were also highly responsive to oxidizing agents (NO_2) and reducing gases (NH_3). Figure 4.3a shows the sensitivity of a MWCNT/AAO device exposed to 100ppm of NH_3 gas. The sensitivities obtained are higher than those reported earlier. The device recorded highest sensitivity of 30.21% to 100 ppm of ammonia gas after 60sec microwave plasma etch of the device at room temperature.

The as prepared sample had a very low sensitivity 0.31% due to the thick a-C layer on top and bottom of the device. An initial 30sec etch on the top side and 30sec etch on the

bottom side have decreased the thickness of the top and bottom a-C layer thus exposing more CNTs to the gas and increasing the sensitivity to 6.24%. After another 30sec plasma etch on the top of the device the sensitivity went high to 30.21%. However another 30sec plasma etch on the bottom side of the device has decreased the thickness of the bottom a-C layer to such an extent that there was a very thin conducting path connecting the CNTs at the bottom, hence the sensitivity has reduced to 8.18%.

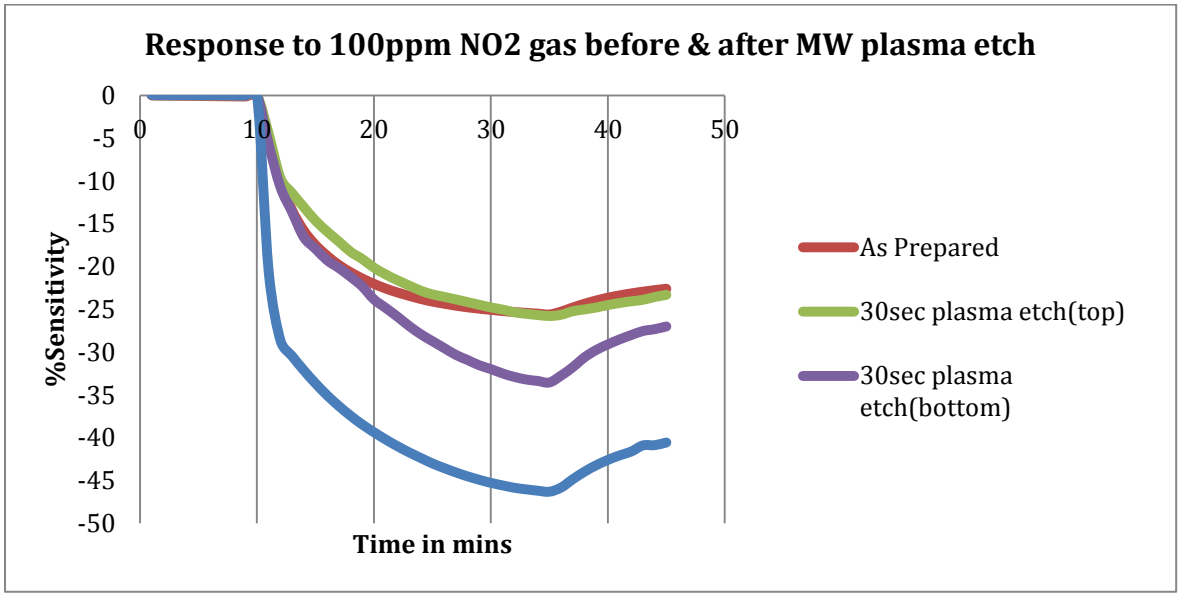

Figure 4.3(b): Steady state response of MWCNT resistive sensor at room temperature at different microwave plasma etch conditions to 100ppm NO_2 gas

Figure 4.3b shows the sensitivity of another sample that recorded highest sensitivity of -46.32% to 100ppm of nitrogen dioxide gas after 60sec microwave plasma etch of the device. The higher sensitivities are also due to the high surface area available for the gas molecules to be adsorbed. The well-defined, highly ordered pores contribute to the high surface area of the MWCNT/AAO based sensor devices.

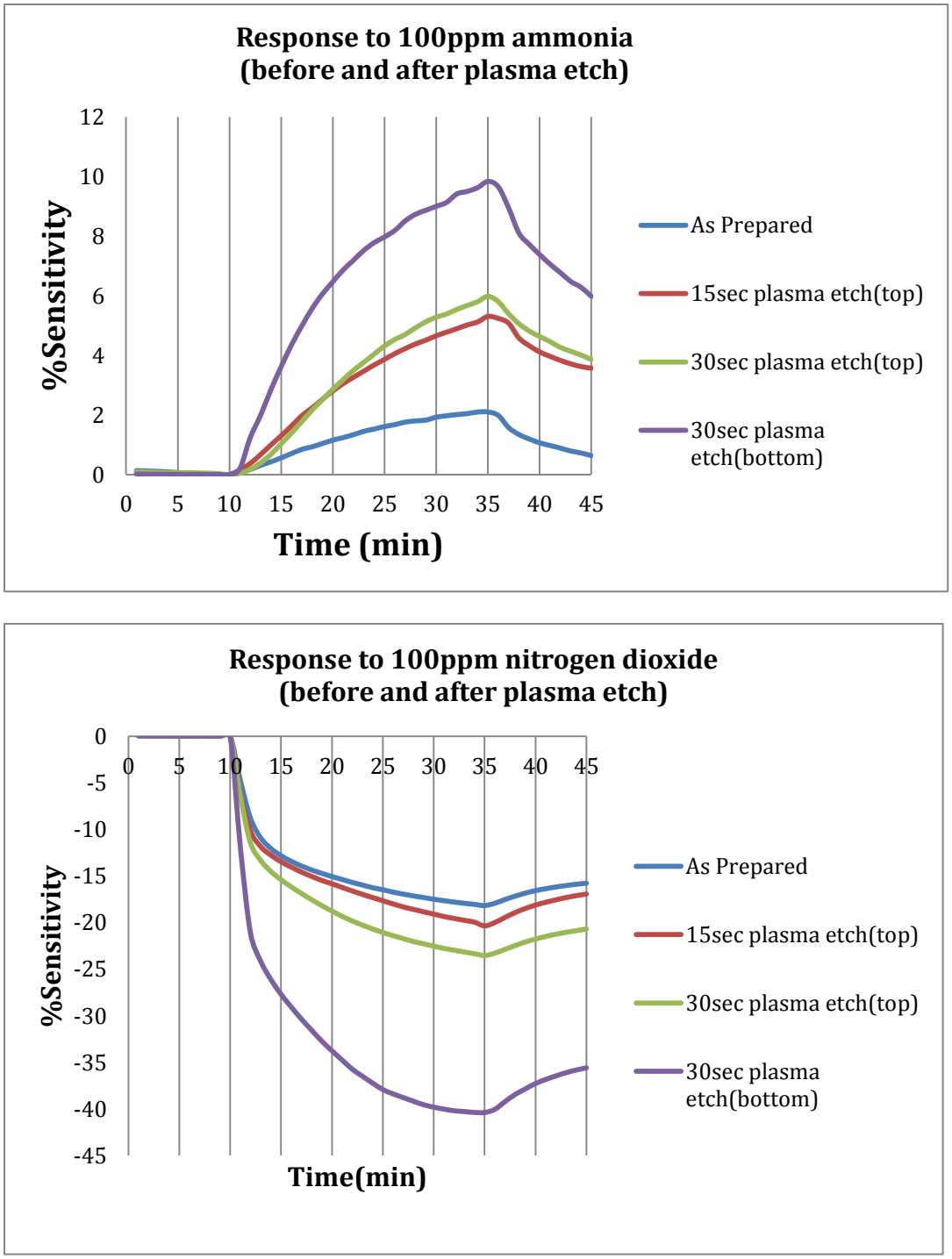

Figure 4.4: Steady state response of another sample at room temperature

Before measuring the sensor response of the sample, the sample was initially exposed to a continuous flow of Nitrogen gas until its resistance reaches a constant value (constant up to 1st decimal place). The baseline resistance of the sample is recorded. For the first

10mins of the sensor response, the sample was exposed to Nitrogen gas as carrier and then we injected the test gas 100 ppm ammonia/nitrogen dioxide gas for the next 25mins until 35mins where peak sensitivity was observed. After 35mins, the gas was switched back to Nitrogen, which was allowed to flow for the next 10mins, after which the gas is turned off.

In case of measuring the sensor responses to ammonia gas, desorption of the analyte gas in the presence of UV light is required. The NH_3 gas molecules are chemisorbed on the MWCNT surface, which causes an upward drift in the baseline resistance as well as the sensitivity. The electrical response of the resistive sensor indicates a charge transfer between the nanotubes and the gas molecules, and hence, the adsorption of gases on the inner walls of the nanotubes is the dominant sensing mechanism. As the sensor goes through $NH_3 – N_2$ cycles there is a accumulation in chemisorbed NH_3 on the MWCNT surface, which causes an upward drift in the baseline resistance as well as the sensitivity. This is due to the fact that the adsorbate binding energy is sufficiently large and some of the ammonia molecules can be adsorbed at the defect sites available either on the nanotubes surface or on the inner walls of the open ended MWCNTs. The gas molecules adsorbed at these defect sites are hard to desorb. Hence, weakly bonded, molecules desorb with each cycle, while the more strongly bonded (chemisorbed or physisorbed at the defect sites) molecules remain during cycling. Binding energy is high enough that heat or ultraviolet light is needed to desorb the analyte and bring the MWCNTs back to its initial conducting state [11].

Figure 4.5(a) and 4.5 (b) show the cyclic response of MWCNT resistive gas sensor where Nitrogen and ammonia/nitrogen dioxide were pumped into the test chamber containing the sample in alternative cycles of 10mins each.

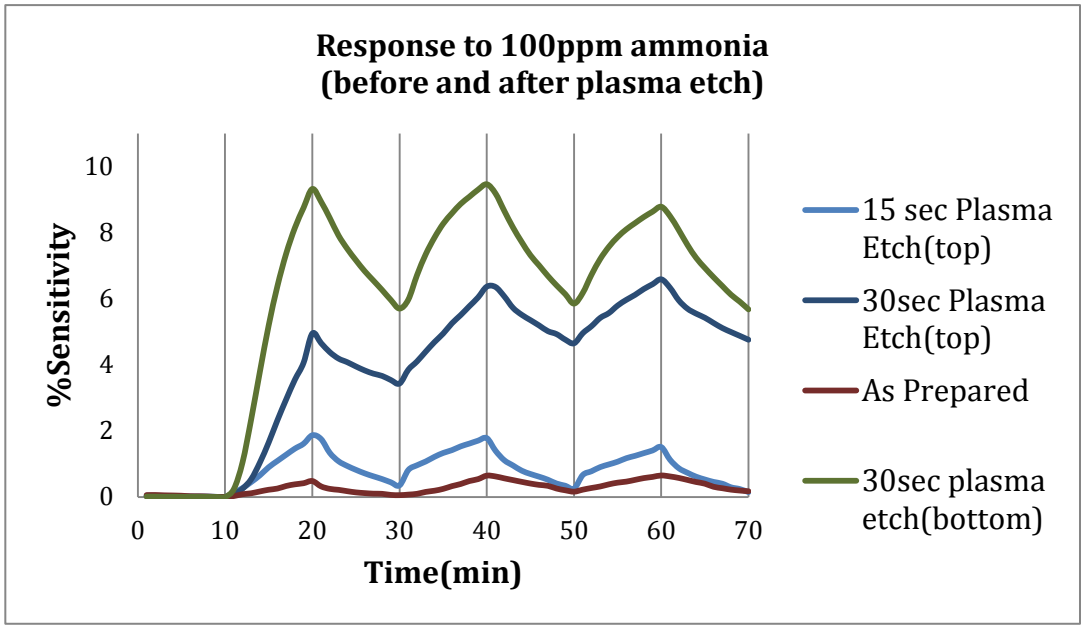

Figure 4.5(a): Response of MWCNTs at different microwave plasma etch conditions to 100ppm NH_3 gas.

The sensor response of a MWCNT/AAO device to 100ppm NH_3 with various a-C layer thicknesses obtained by plasma oxidation technique is shown in Figure 4.5. The initial response corresponds to as prepared sample with an a-C layer thickness of 20nm. The Baseline resistance was 30.8 Kilo ohms with 0.87% cumulative sensitivity to ammonia. Then the sample was oxygen plasma oxidized for 15 sec to decrease the a-C layer thickness to 8nm and the corresponding sensor response is shown in Figure 4.5. The baseline resistance and the cumulative sensitivity were increased to 60.1 Kilo Ohms and 1.686% respectively. The sample was further plasma oxidized for another 15 sec which

yielded a sensor response with baseline resistance increased to 70 kilo Ohms a cumulative sensitivity of 6.5% was observed.

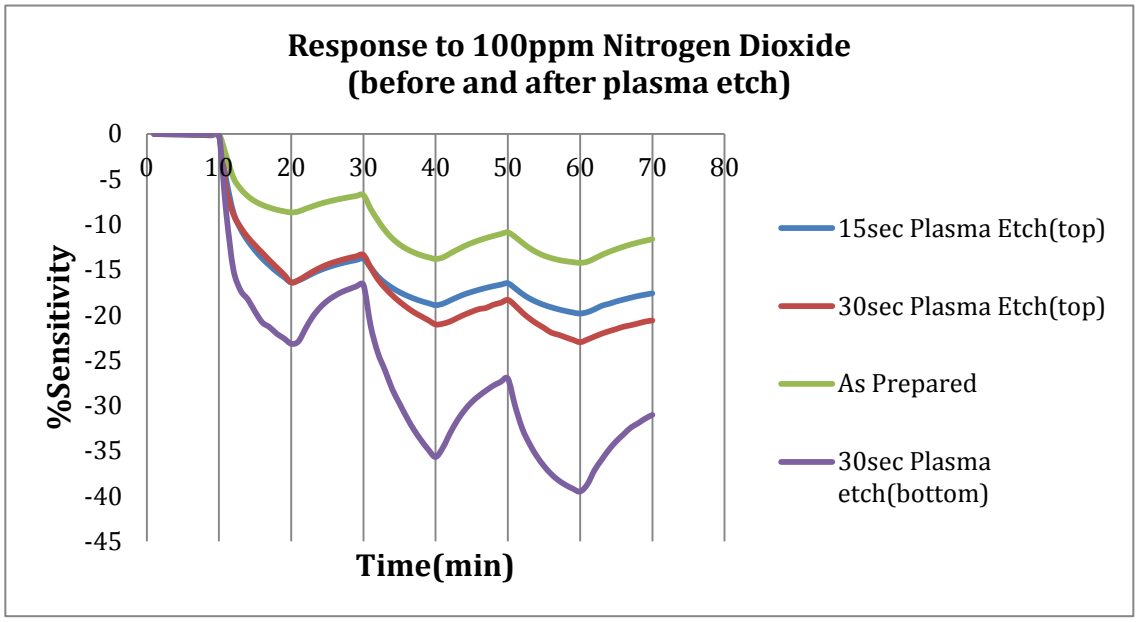

Figure 4.5(b): Response of MWCNTs at different microwave plasma etch conditions to 100ppm NO_2 gas

As seen in Figure 4.5(b), the as prepared sample had a device baseline resistance of 57.9K ohm and a sensitivity of -16.4%. After 30sec plasma etch on top and 30sec plasma etch on bottom the baseline resistance and sensitivity of the device had increased to 131.35K ohm and -23.16% respectively.

The increase in baseline resistance and device sensitivity with decreasing a-C layer thickness was found in agreement with the previous experimental results. These results underline the important role played by the amorphous carbon layer as a conducting contact between the adjacent CNTs, even though the primary sensing mechanism involves the interaction of the carbon nanotubes with the analyte.

Table 4.1and Table 4.2 summarize the results of different plasma etch conditions.

Table 4.1: Response to 100ppm Ammonia Gas at different Microwave Plasma Etch Conditions

Sample name	**Condition**	**Baseline Resistance**	**%Sensitivity**
SSMWCNT01	As Prepared	11.93K ohm	0.31
	30 sec Plasma Etch (top)	12.58K ohm	0.32
	30 sec Plasma Etch (bottom)	174.76K ohm	6.24
	60sec Plasma etch (top)	233.62K ohm	30.21
	60 sec Plasma Etch (bottom)	388.16K ohm	8.01
SSMWCNT02A	As Prepared	39.12K ohm	2.1
	15sec Plasma Etch (top)	59.77K ohm	5.3
	30sec Plasma Etch (top)	66.61K ohm	5.98
	60sec Plasma Etch (bottom)	125.98K ohm	9.84
SSMWCNT02B	As Prepared	30.84K ohm	4.37
	15sec Plasma Etch (top)	29.13K ohm	10.56
	30sec Plasma Etch (top)	32.76K ohm	11.1
	60sec Plasma Etch (bottom)	169.05K ohm	11.5

Table 4.2: Response to 100ppm Nitrogen Dioxide Gas at different Microwave Plasma Etch Conditions

Sample name	**Condition**	**Baseline Resistance**	**%Sensitivity**
SSMWCNT01	As Prepared	31.5 K ohm	-25.6
	30 sec Plasma Etch(top)	36.17 K ohm	-25.78
	30 sec Plasma Etch (bottom)	175.73 K ohm	-33.55
	60sec Plasma etch (top)	309.65 K ohm	-46.2
	60 sec Plasma Etch (bottom)	388.24 K ohm	38.26
SSMWCNT02A	As Prepared	39.72K ohm	-18.16
	15sec Plasma Etch(top)	61.96K ohm	-20.34
	30sec Plasma Etch(top)	68.71K ohm	-23.5
	30sec Plasma Etch(bottom)	138.92K ohm	-40.38
SSMWCNT02B	As Prepared	30.23K ohm	-25.5
	15sec Plasma Etch(top)	31.53K ohm	-22.84
	30sec Plasma Etch(top)	36.17K ohm	-25.78
	30sec Plasma Etch(bottom)	175.73K ohm	-30.7

4.3 MWCNT-Metal Nanoparticle gas sensors

The a-C layer has a resistivity of $3.75*10^{-5}$ohm-m, so when it is replaced with a metal layer with less resistivity the MWCNT resistive sensor would yield a sensor response of higher sensitivity and low response time. This chapter includes the experimental results proving the above fact. We have chosen three metals in our present work, namely Au, Ni and Cu. However when these metals are sputtered on the MWCNT resistive sensor device they do not form a continuous layer of finite thickness, instead they form small

clusters on the surface. Many types of metals do not form continuous structures on the nanotube surface because of a weaker metal-carbon interaction, thus leading to the formation of isolated metal nanoclusters on the CNT surface. The key concept is the use of relatively small clusters that donate or accept a significant amount of charge upon adsorption of a target molecule. These MWCNT-metal nanocluster surfaces serve as reactive sites for gas adsorption.

Theoretical works and experimental results indicate that metallic clusters strongly interact with CNTs producing significant charge reorganization. Therefore, another way to exploit the high sensitivity of CNTs is the creation of nanotube–metal cluster assemblies. Moreover, these clusters can be mechanically and chemically robust and stable, and hence, compared to polymer-based sensors, metal-based sensors can operate at higher temperatures and in harsher environments [12].

The MWCNT resistive sensors gave high sensitivities according to Table 4.1 and 4.2 to ammonia and nitrogen dioxide gases with the decreasing thickness of a-C layer. After removing the a-C layer and sputtering the top side with metal of higher work function than that of CNTs, the sensitivity would decrease because the current directly flowed through the direct path between the bus bars of the CNTs without involving the CNTs. However when the metal is sputtered on the back side of the device, the sensitivity would increase because this sputtered metal behaved as a conducting layer between the CNTs of the model through which the current can pass through the alternate path through the CNTs. Since the metal nano clusters result in relatively more charge transfer upon

adsorption of the target gas they theoretically give more sensitivity than pristine MWCNTs. The sensitivity would also decrease with the increasing thickness of the metal layer as the pores of the template will be blocked by the metal layer, thereby decreasing the availability of CNT sites for adsorption of the ammonia molecules.

When we replaces the value of resistivity of the a-C layer with the resistivity of the metal in our simulation model developed to calculate the device resistance, the model would give the practical values obtained for the device resistance with a deviation. The deviation from measured values was mainly because the sputtered film of metal was not continuous and of the exact thickness of 5 nm as we sputtered.

According to the basic theory of metal/semiconductor interface, the p-type semiconducting CNT can form an ohmic contact with a metallic electrode when $\varphi M > \varphi S$, where φM and φS are the work functions of the metallic electrode and the semiconducting CNT, respectively. On the other hand, a metallic electrode having a lower work function than φS may form a schottky barrier at the metal/CNT contact. In contrast to this, the n-type semiconducting CNT could form the schottky barrier when $\varphi M > \varphi S$ [13]. The work function of Au, Ni and Cu are 5.1eV, 5.04eV and 4.53eV respectively. The work function of CNT according to literature is approximately equal to 4.4eV, which decreases after plasma etching steps to 4.2eV [14-16]. Clearly the work function of the metals we chose is higher than that of the CNTs, hence the metals would form a ohmic contact with the CNTs. The sensor response after the metal sputtering also shows that the CNTs show p-type behaviour.

4.3.1 Au sputtering results:

Figure 4.6 shows the SEM image of the Au nano clusters deposited by rf-sputtering onto MWCNT resistive sensor. Although our intention was to deposit a uniform thick layer of 5nm, the rf-sputtering results in the formation of nano clusters on the surface of the device.

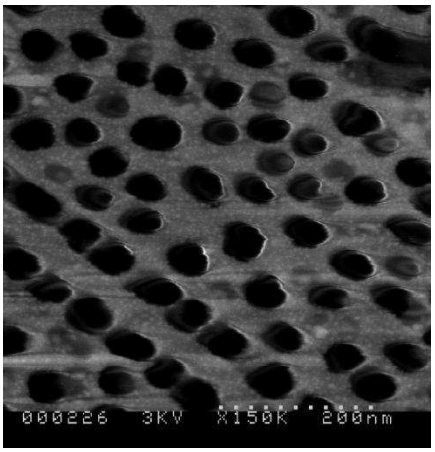

Figure 4.6: SEM image of the Au nano clusters deposited by rf-sputtering onto MWCNT resistive sensor.

The rational modification of the CNTs surface with Au nanoclusters enables nanotubes with tunable surface properties for the fabrication of selective gas sensors. Au particles on the nanotubes strongly affect their properties of gas adsorption, hence, the tailoring of gas sensitivity. The Au metal in the form of thin film is the only metal, is inert in oxygen atmosphere and excludes influence of this interfering gas on the sensor response. In the contrast, Au nanoparticles are catalytically active, even at ambient temperature, and could increase the selectivity of the chemical reactions involved for detecting toxic gases. This enhanced catalytic activity of the Au nanoparticles depends on their size, at nanoscale effects [17].

Figure 4.7(a) shows the steady state sensing curves of the MWCNT sensor, unmodified and functionalized with various Au nanoclusters, exposed to 100ppm NH_3, at room temperature.

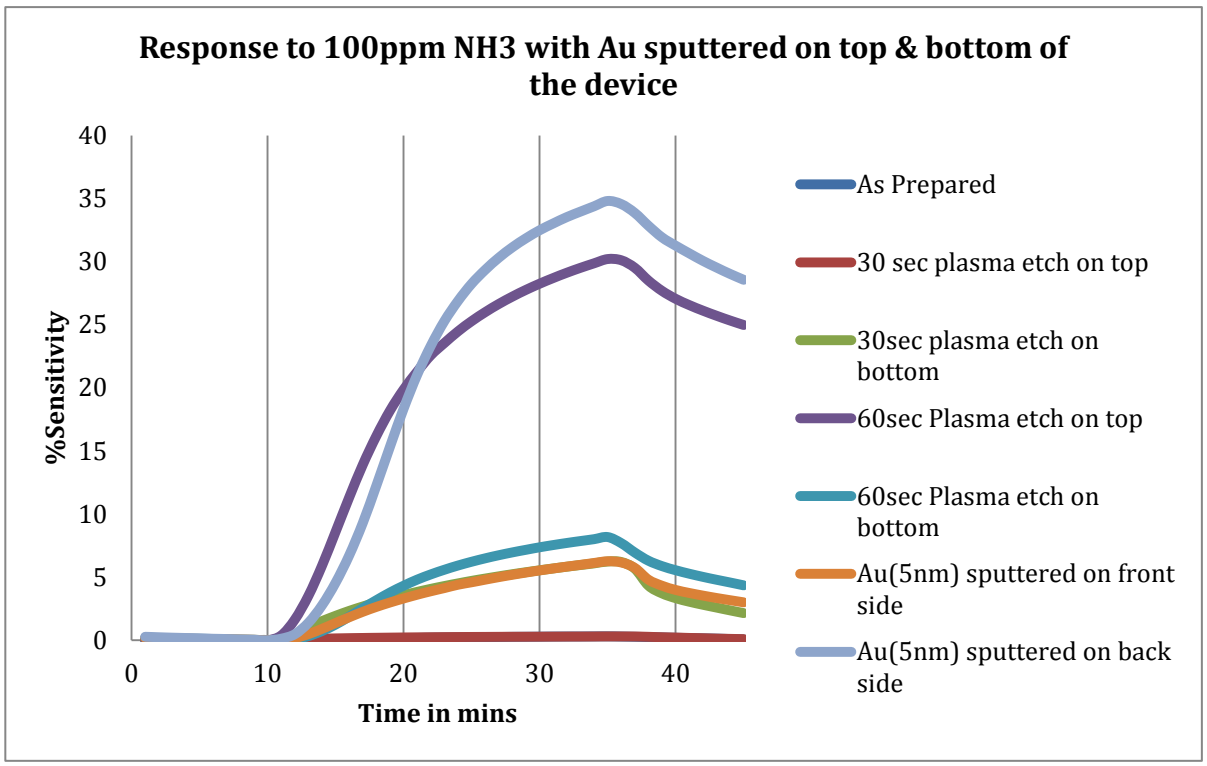

Figure 4.7(a): Response of unmodified MWCNT and MWCNTs functionalized with various Au nanoclusters to 100ppm NH_3

The as prepared sample had a device baseline resistance of 11.93 Kilo ohm and a sensitivity of 0.31%. After series of microwave plasma etches (60seconds of plasma etch on top and 60seconds on bottom) as shown in Figure 4.7(a) the device had a baseline resistance of 388.16K ohm and a sensitivity of 8.18%. After sputtering the top side of the device with Au of 5nm thickness, the device sensitivity drastically decreased to 6.26%. This is because the sputtered metal would form the direct current path between the electrodes without involving the CNTs. After sputtering the bottom side of the device with Au of 5nm thickness the device sensitivity increased to 34.82%. The metal sputtered

on the bottom side of the device would provide a conducting layer between the CNTs, thus involving more number of CNTs in the response, this way the current through the alternate current path would increase which therefore increases the sensitivity of the device. The sensitivity (34.82%) of MWCNTs functionalized with Au particles is much more than the sensitivity (8.18%) of MWCNTs without any functionalization.

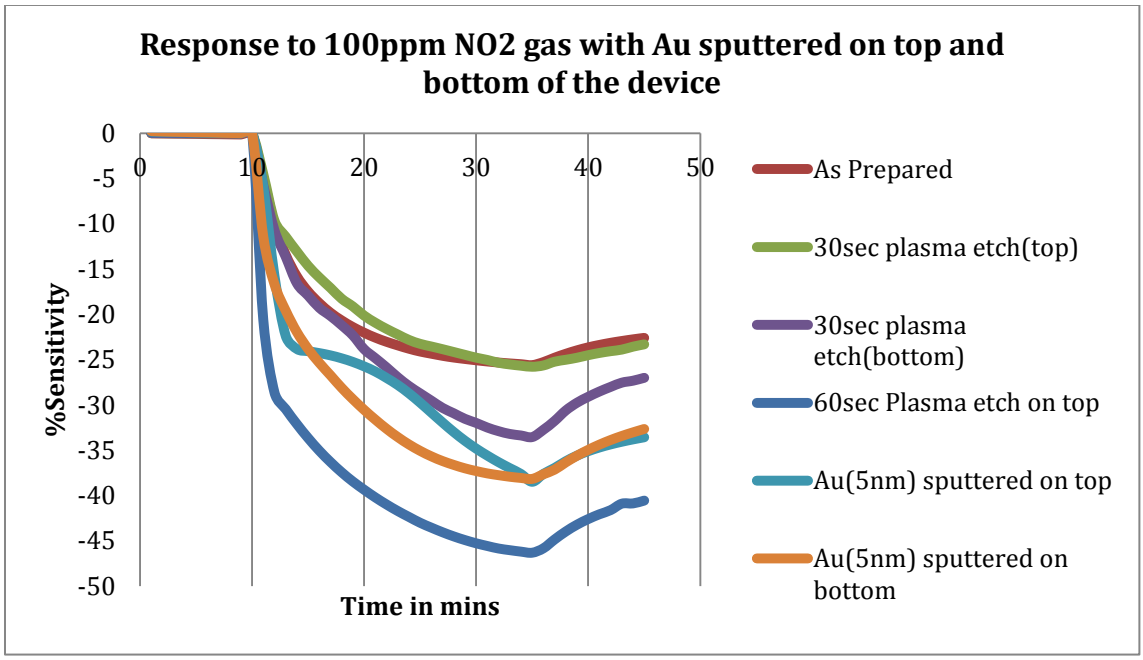

Figure 4.7(b): Response of MWCNT resistive sensor to 100ppm NO_2 with Au sputtered on top and bottom sides of the device

Figure 4.7(b) shows the response of the device to 100ppm NO_2 with Au sputtered on top and back sides of the device. In this case, the as prepared sample had a sensitivity of 25.4% which increased to 30% after the plasma etching steps as listed in Figure 4.7(b). After sputtering Au on the top and bottom the device sensitivity increased to 38.1%. Clearly the results suggest that when the sensors are exposed to the analyte gas (ammonia/nitrogen dioxide), both the MWCNT and the metallic nanoclusters interact with the gas. However, metal nanoclusters seem very reactive to the analyte gas. Upon

adsorption of a gas molecule, there is a significant charge transfer between the metallic nano-cluster and the nanotube, which results in a measurable change in the overall conductance of the active film. This effect is much stronger than the one caused by the direct interaction of the analyte gas and the carbon nanotube wall, since the responsiveness of bare MWCNT sensors is lower than the one of metal-decorated MWCNT sensors [18].

Table 4.3: Results of Au sputtered sample when exposed to 100 ppm ammonia.

Condition	**Baseline Resistance**	**%Sensitivity**
As prepared	11.93K ohm	0.31
30sec plasma etch on top	12.58K ohm	0.32
30sec plasma etch on bottom	174.76K ohm	6.24
60sec plasma etch on top	233.62K ohm	30.21
60sec plasma etch on bottom	388.16K ohm	8.01
Au(5nm) on top	426.21K ohm	6.26
Au(5nm) on bottom	339.03K ohm	34.82

Table 4.4: Results of Au sputtered sample when exposed to 100 ppm nitrogen dioxide.

Condition	Baseline Resistance	%Sensitivity
As prepared	31.5 K ohm	-25.6
30sec plasma etch on top	36.17K ohm	-25.78
30sec plasma etch on bottom	175.73 K ohm	-33.55
60sec plasma etch on top	309.65 K ohm	-46.2
60sec plasma etch on bottom	388.24 K ohm	-38.26
Au(5nm) on top	435.96K ohm	-38.16
Au(5nm) on bottom	412.16K ohm	-38.48

4.3.2 Cu sputtering results:

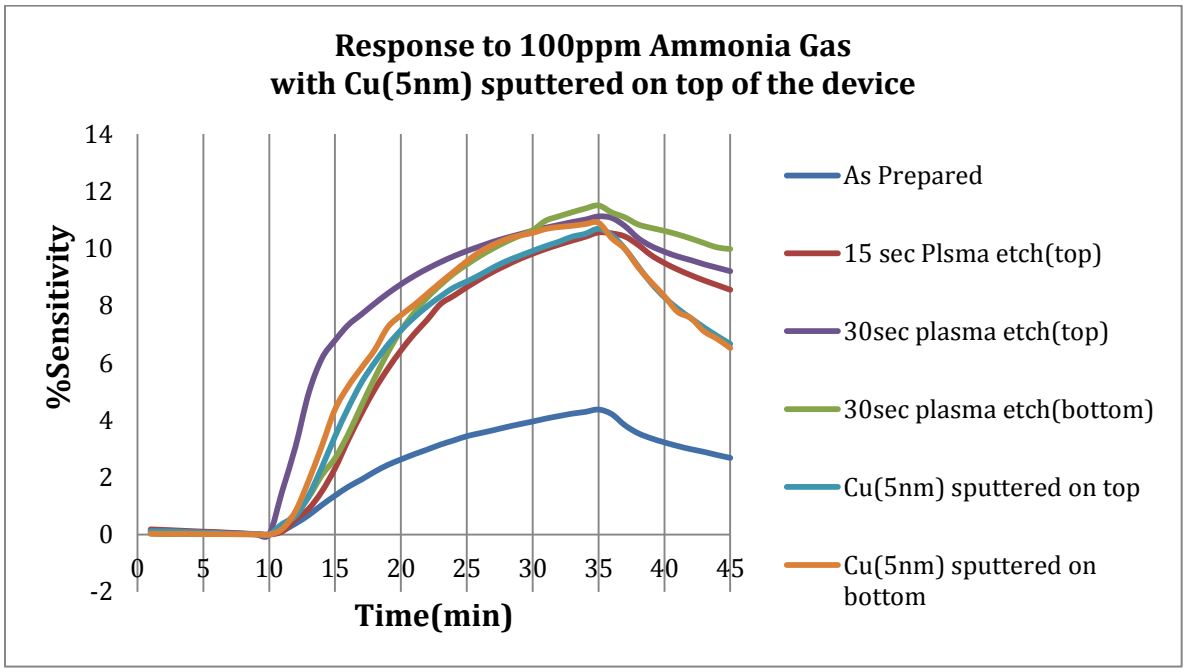

Figure 4.8(a): Steady state sensor response of MWCNT-Cu sensor to 100ppm ammonia.

Table 4.5: Results of Cu sputtered sample when exposed to 100 ppm ammonia.

Condition	**Baseline Resistance**	**%Sensitivity**
As prepared	30.84K ohm	4.37
15sec plasma etch on top	29.13K ohm	10.56
30sec plasma etch on bottom	32.76K ohm	11.1
30sec plasma etch on bottom	169.05K ohm	11.5
Cu (5nm) on top	112.25K ohm	10.69
Cu (5nm) on bottom	65.6K ohm	10.89

After removing the a-C layer and depositing the metal layer on the top of the device, it is seen that the device baseline resistance decreases and so does its sensitivity. The sensitivity decreases because the metal layer forms a direct current path between the electrodes without involving the CNTs. It is seen that after depositing a metal layer on the bottom of the device the sensitivity increases because the metal layer facilitates flow of current through the CNTs.

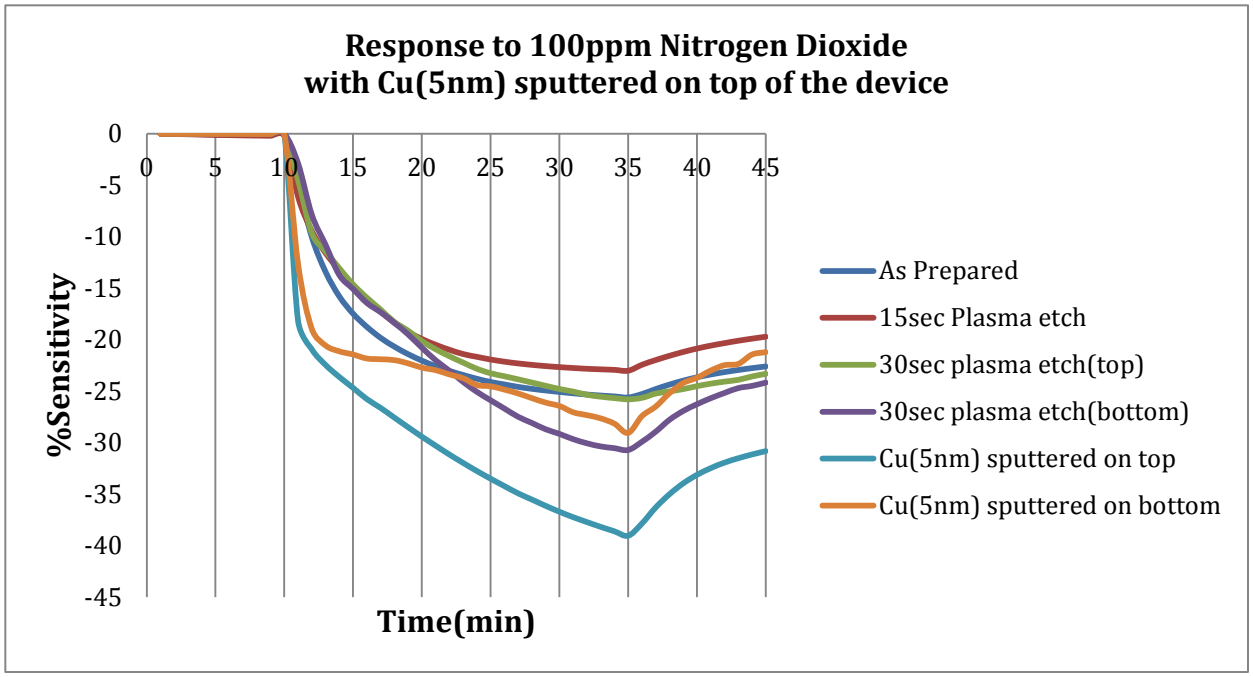

Figure 4.8(b): Steady state sensor response of MWCNT-Cu sensor to 100ppm nitrogen dioxide.

Table 4.6: Results of Cu sputtered sample when exposed to 100 ppm nitrogen dioxide.

Condition	**Baseline Resistance**	**%Sensitivity**
As prepared	30.23K ohm	-25.5
15sec plasma etch on top	31.53K ohm	-22.84
30sec plasma etch on bottom	36.17K ohm	-25.78
30sec plasma etch on bottom	175.73K ohm	-30.7
Cu (5nm) on top	649.05K ohm	-39.02
Cu (5nm) on bottom	289.72K ohm	-29.04

Is is seen that after depositing Cu layer of 5nm on the bottom of the device the sensitivity of the device decreased (-29.04%) when exposed to 100ppm nitrogen dioxide gas but

increased (10.89%) when exposed to 100ppm ammonia gas. Hence Cu metal layer on MWCNT make the device selective to reducing gases such as ammonia.

Figures 4.9(a) and 4.9(b) show the cyclic response of Cu-MWCNT resistive sensor to 100ppm of ammonia and 100ppm of nitrogen dioxide respectively.

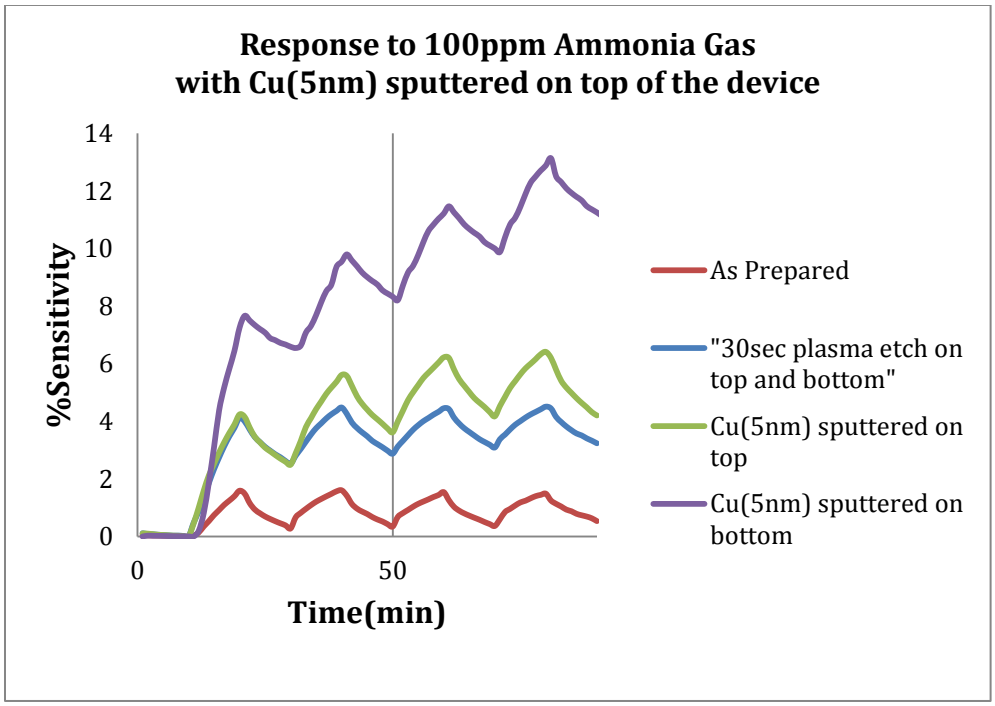

Figure 4.9(a): Cyclic response of Cu-MWCNT to 100ppm ammonia

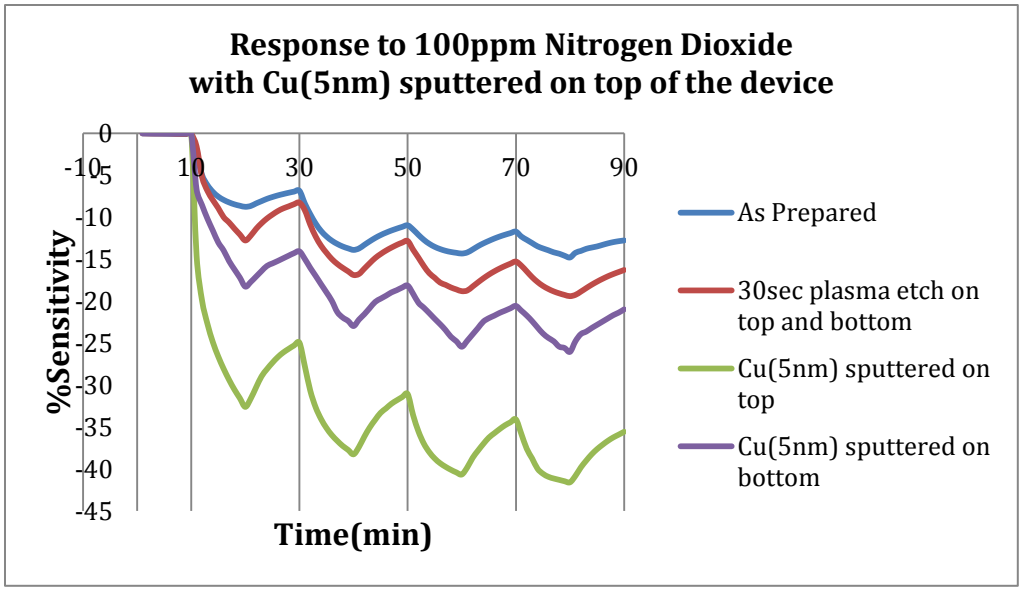

Figure 4.9(b): Cyclic response of Cu-MWCNT to 100ppm nitrogen dioxide

4.3.3 Ni sputtering results:

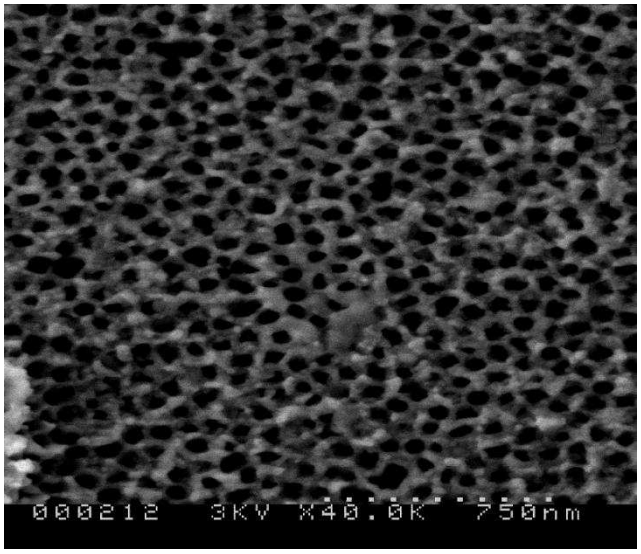

Figure 4.10: SEM image of the Ni nano clusters deposited by rf-sputtering onto MWCNT resistive sensor.

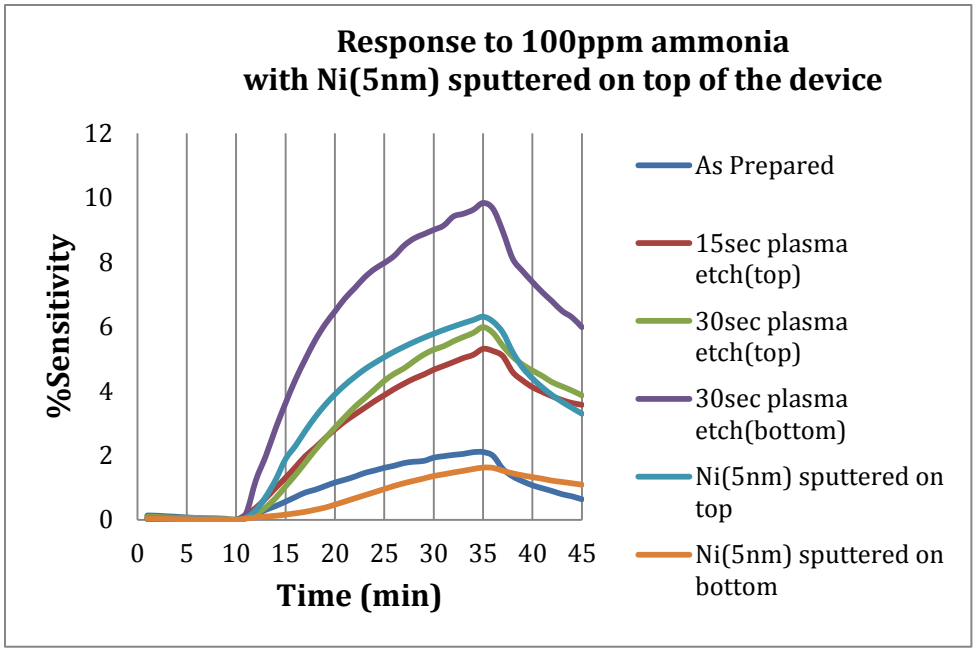

Figure 4.11(a): Steady state sensor response of MWCNT-Ni sensor to 100ppm ammonia.

Table 4.7: Results of Ni sputtered sample when exposed to 100 ppm ammonia.

Condition	**Baseline Resistance**	**%Sensitivity**
As prepared	39.12K ohm	2.1
15sec plasma etch on top	59.77K ohm	5.31
30sec plasma etch on top	66.61K ohm	5.98
30sec plasma etch on bottom	125.98K ohm	9.84
Ni(5nm) on top	16.79K ohm	6.31
Ni(5nm) on bottom	2.26K ohm	1.62

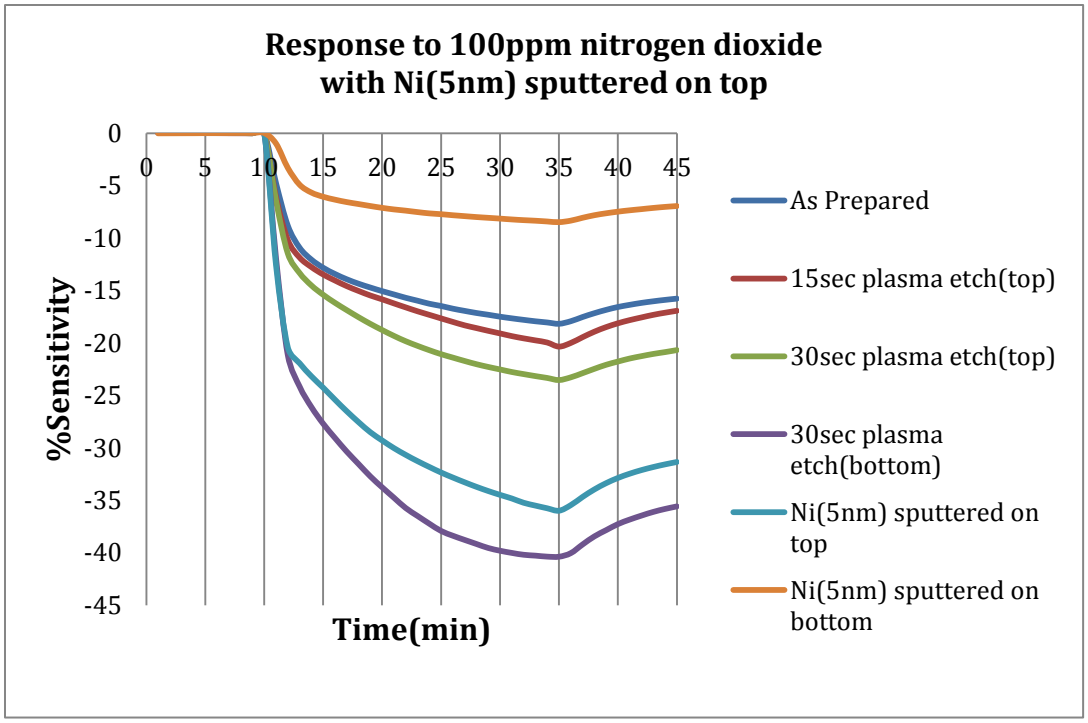

Figure 4.11(b): Steady state sensor response of MWCNT-Ni sensor to 100ppm ammonia.

Table 4.8: Results of Ni sputtered sample when exposed to 100 ppm nitrogen dioxide.

Condition	**Baseline Resistance**	**%Sensitivity**
As prepared	39.72K ohm	-18.16
15sec plasma etch on top	61.96K ohm	-20.34
30sec plasma etch on top	68.71K ohm	-23.53
30sec plasma etch on bottom	138.92K ohm	-40.38
Ni(5nm) on top	41.52K ohm	-35.99
Ni(5nm) on bottom	2.48K ohm	-8.47

Figures 4.12(a) and 4.12(b) show the cyclic response of Ni-MWCNT resistive sensor to 100ppm of ammonia and 100ppm of nitrogen dioxide respectively.

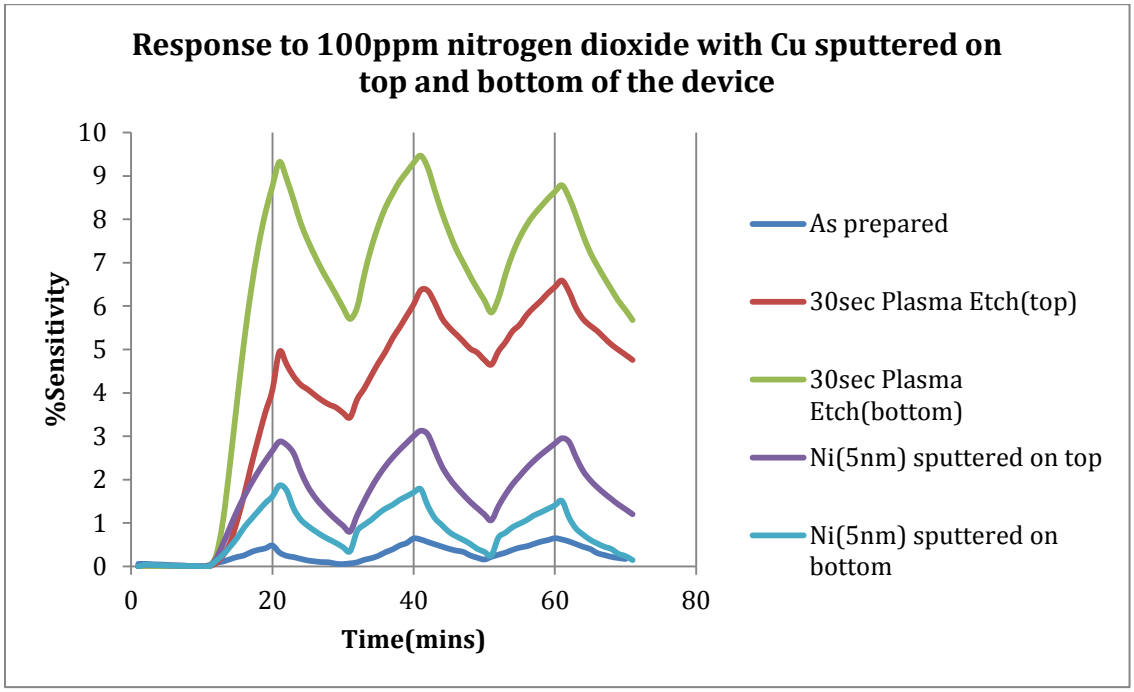

Figure 4.12(a): Cyclic response of MWCNT-Ni to 100ppm ammonia gas

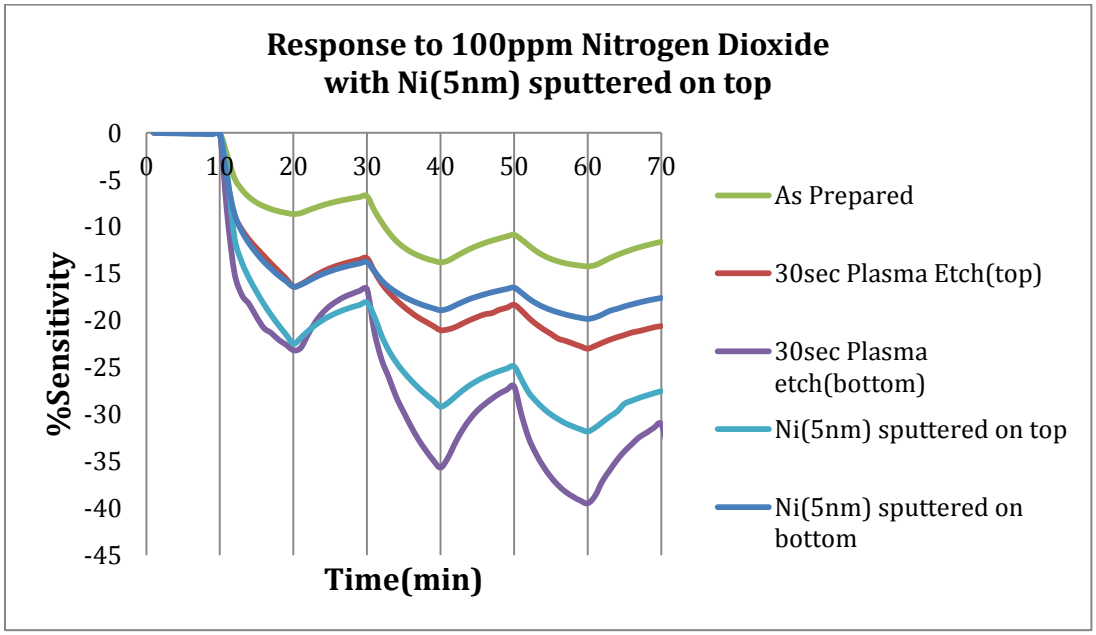

Figure 4.12(b): Cyclic response of MWCNT-Ni to 100ppm nitrogen dioxide gas

4.4 Comparison of Au, Cu and Ni sputtering results

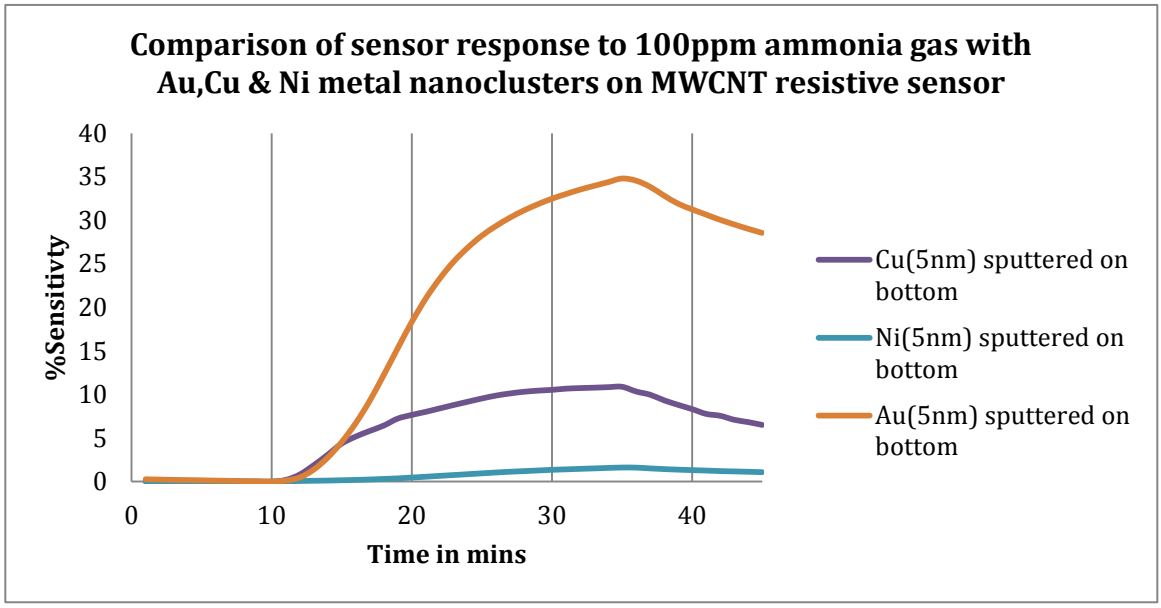

Figure 4.13: Comparison of Au, Cu and Ni sputtering results in presence of 100ppm ammonia gas after depositing 5nm on back side

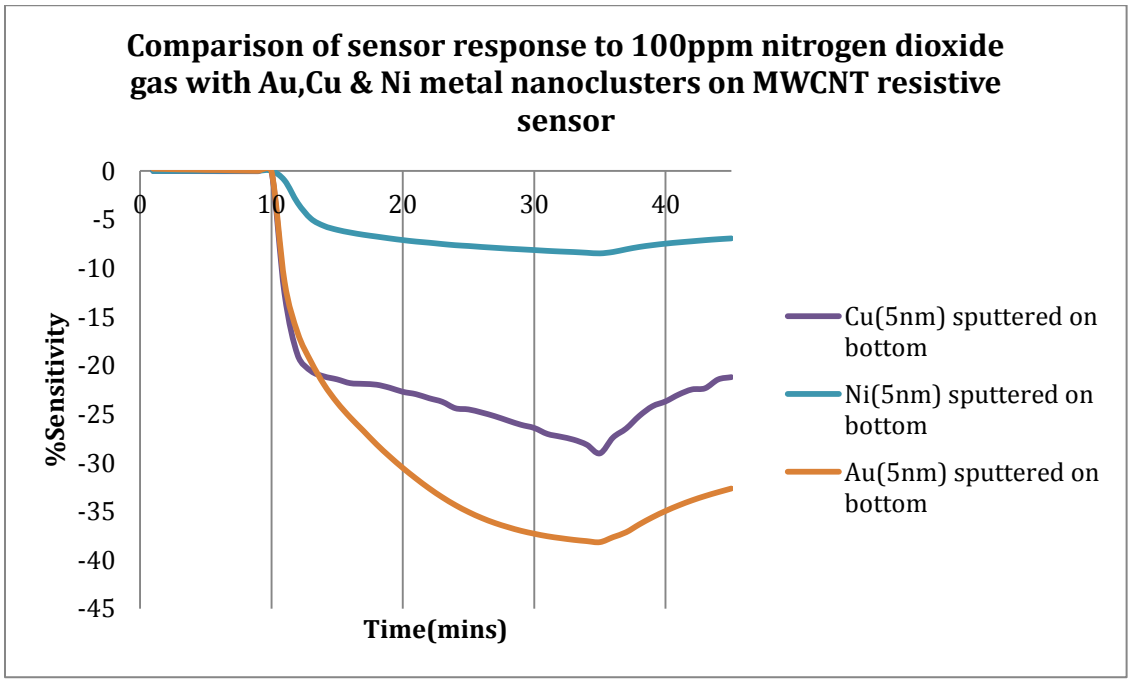

Figure 4.14: Comparison of Au, Cu and Ni sputtering results in presence of 100ppm nitrogen dioxide gas after depositing 5nm on back side

Table 4.9 shows the comparison of the work function of the metal on the device and its sensitivity to 100ppm ammonia and 100ppm nitrogen dioxide with metal deposited on top and bottom sides of the device.

Table 4.9: Comparison of work function of metals and the sensitivities obtained

Work Function(ϕ) eV	**%S to 100ppm ammonia**	**%S to 100ppm nitrogen dioxide**
Au 5.1eV	34.82	-38.48
Ni 5.04eV	1.62	-8.47
Cu 4.53	10.89	-29.04

It is clear that MWCNTs with Au nanoclusters exhibit better sensitivity to ammonia and nitrogen dioxide gases, than that with Ni or Cu nanoclusters. This is because Ni and Cu nanoclusters are not inert to oxygen and readily oxidize in air to form compounds which may have different work functions different from the ideal values, that do not give the desired response. Au nanoclusters are inert in air, which explains the high sensitivity compared to other metals.

4.5 Implementing the resistive sensor model for calculating the device resistance with metal sputtered

Table 2.2 shows the final values of thickness of top and bottom a-C layers. Before sputtering metal on one side of the device, the a-C layer is completely etched off and the other side has the a-C layer of thickness as shown in Table 2.2. The a-C layer on the other side is also etched off before sputtering the metal. The baseline resistance measured for each device with metal layer sputtered on top and bottom sides of the device is measured

and compared with the value calculated from the model. The resistivity of Au, Cu and Ni used in model are 22.14nΩ-m [19], 16.78nΩ-m [20] and 69.3nΩ-m [21] respectively. Table 4.9 shows the measured and calculated values of baseline resistance of the device.

Table 4.10: Simulation results for calculating R_{dev} with metal layer on top and bottom

Metal	**Ttop(nm)**	**Tbot(nm)**	**Rdev (measured)**	**Rbase (calculated)**	**LSE (Rdev-Rbase)^2**
Au(top)	0.009	0.001	425.99K ohm	426.21 K ohm	4.8*10^-2
Au(bottom)	0.009	0.004	339 K ohm	339.03 K ohm	9*10^-4
Cu(top)	0.026	0.001	112.12 K ohm	112.25 K ohm	1.7*10^-2
Cu(bottom)	0.026	0.02	65.62 K ohm	65.61K ohm	1*10^-4
Ni(top)	0.41	0.33	16.8 K ohm	16.79 K ohm	1*10^-4
Ni(bottom)	4.8	0.33	2.27 K ohm	2.26 K ohm	1*10^-4

Chapter 5: Conclusion and scope of future work

Vertically aligned MWCNTs were grown in the highly ordered pores of alumina templates through CVD process. The MWCNTs grown in the templates are resistive sensors with p-type semiconductor nature. An excellent response to low concentration of 100ppm of ammonia and 100ppm nitrogen dioxide was observed. The effect of the a-C layer formed as a byproduct of CVD process, on the device baseline resistance and sensitivity was studied with the help of the theoretical model developed [22].This model was necessary to understand the change in the current path with decrease in thickness of a-C layer and also suggest the device configuration to obtain the highest sensor response. The design for the device configuration should be such that the current is made to flow through the alternate path by tailoring the thickness of a-C layer. The simulation model obtained for calculating the device resistance matched with the measured values of device resistance. A model to calculate the change of device resistance with respect to the number of gas molecules was also developed. The values of resistance of CNTs, top and bottom a-C layers were obtained by the simulation model which was in accord with measured experimental values of resistance.

The effect of microwave plasma etch of the a-C layer on the sensitivity of MWCNT resistive sensor was also studied. Microwave plasma etch was done at a power of 75W, at room temperature. Plasma etch decreases the thickness of a-C layer, which enhances the sensitivity of the device. However, these CNTs do also get functionalized with oxygen groups in this plasma etching process which changes the binding energy at the tips of the CNTs which is responsible for giving a better response to ammonia molecules.

We obtained a very high steady state sensitivity of 30.21 % to 100ppm ammonia and -46.32% to 100ppm nitrogen dioxide gases. All the sensing measurements were done at room temperature and relative humidity of about less than 10 %.

Removing the a-C layer fully and then replacing it with a more conductive layer like metal nanocluster can be expected to give a better response and enhance the sensitivity of the sensor which was observed in the results of metal sputtering experiments. The three metals (Au, Cu and Ni) formed ohmic contacts with the CNT layer , which behaved as a p-type semiconductor layer. Sensitivities to 100 ppm ammonia recorded after Au, Cu and Ni deposition of 5 nm on the back side of the template were 34.82%, 10.89% and 1.62% respectively as shown in Figure 4.13. Sensitivities to 100 ppm nitrogen dioxide recorded after Au, Cu and Ni deposition of 5 nm on the back side of the template were -38.17%, -29.04% and -8.47% respectively as shown in Figure 4.14. This experiment also helped in understanding the current flow path of the model and its relation to the sensitivity of the device. The current flow path optimization of the model was necessary to get the highest sensor response. This was accomplished by making the current choose the alternate path through the MWCNTs. To achieve this, we made the direct current path too resistive by decreasing the a-C layer thickness. Note that the thickness of a-C layer is inversely proportional to resistance of the top and bottom layers of a-C.

Many other plasma etching techniques like PECVD etch, water plasma etch can be studied in detail. Also all the etching techniques can be tested in various atmospheres like water plasma or argon. Detailed study can be done on plasma etching techniques of how the sensor binding energy and work function are changed with respect to the removal of a-C layer. This would also help us to find out new techniques to remove a-C layer. Also,

functionalization of the CNTs with metal nanoclusters is underway to improve the sensitivity and develop a better sensor.

References

[1]. M. Penza, R. Rossi, M. Alvisi, G. Cassano, M. A. Signore, E. Serra, and R. Giorgi, "Surface Modification of Carbon Nanotube Networked Films with Au Nanoclusters for Enhanced NO_2 Gas Sensing Applications".

[2]. Radouane Leghriba, Roman Pavelkoa, "Gas sensors based on multiwall carbon nanotubes decorated with tin oxide nanoclusters".

[3] Shripriya Poduri, Dr. Vijay Singh, "Theoretical modeling and analysis of ammonia gas sensing properties of vertically aligned MWCNTs resistive sensors and enhancing their sensitivity".

[4]. Patricia A Clore Thesis, University of Kentucky, 2008,6-11

[5] Ting Zhang, Syed Mubeen, Nosang V Myung and Marc A Deshusses, "Recent progress in carbon nanotube-based gas sensors".

[6] Hyunju Chang, Jae Do Lee, Seung Mi Leeb and Young Hee Lee, "Adsorption of NH_3 and NO_2 molecules on carbon nanotubes".

[7] Masashi Shiraishi, Koichiro Hinokuma and Masafumi Ata, 2000 American Institute of Physics 1-56396-973-4/007

[8] Peng Liu, Yang Wei, Kaili Jiang, Qin Sun, Xiaobo Zhang, and Shoushan Fan, PHYSICAL REVIEW B **73**, 235412 _2006

[9**]** Hiroki Ago,Thomas Kugler, Franco Cacialli, William R. Salaneck, Milo S. P.Shaffer,Alan H. Windle, and Richard H. Friend, J. Phys. Chem. B 1999, 103, 8116-8121

[10] Properties of Amorphous Carbon, Publisher: Institution of Engineering and Technology Copyright © 2003, Edited by: Silva, S. Ravi P.

[11] Raghu Mangu Thesis,University of Kentucky, December 2008,56

[12]. A Goldoni, L Petaccia, S Lizzit and R Larciprete, "Sensing gases with carbon nanotubes: a review of the actual situation".

[13] Masashi Shiraishi, Koichiro Hinokuma and Masafumi Ata , 2000 American Institute of Physics 1-56396-973-4/007

[14] Peng Liu, Yang Wei, Kaili Jiang, Qin Sun, Xiaobo Zhang, and Shoushan Fan, PHYSICAL REVIEW B **73**, 235412 _2006

[15**]** Hiroki Ago,Thomas Kugler, Franco Cacialli, William R. Salaneck, Milo S. P. Shaffer,Alan H. Windle, and Richard H. Friend, J. Phys. Chem. B 1999, 103, 8116-8121

[16] Patricia A Clore Thesis, University of Kentucky, 2008,6-11

[17]. M. Penzaa, R. Rossia, M. Alvisia, G. Cassanoa, E. Serra, "Functional characterization of carbon nanotube networked films functionalized with tuned loading of Au nanoclusters for gas sensing applications".

[18]. E.H. Espinosa, R. Ionescu, C. Bittencourt, A. Felten, R. Erni, G. Van Tendeloo, J.-J. Pireaux, E.Llobet, "Metal-decorated multi-wall carbon nanotubes for low temperature gas sensing".

[19]. http://en.wikipedia.org/wiki/Gold

[20]. http://en.wikipedia.org/wiki/Copper

[21]. http://en.wikipedia.org/wiki/Nickel

[22]. Raghu Mangu, Suresh Rajaputra, Patricia Clore, Dali Qian, Rodney Andrews and Vijay P. Singh, Materials Science and Engineering: B, 19 March 2010, 19 (2008) 345502

Vita

Swetha Sree Nimmagadda was born in Hyderabad, Andhra Pradesh, India on October 19, 1986. After completing Bachelor of Technology in Electrical and Electronics Engineering from Sreenidhi Institute of Science and Technology, Hyderabad, India, in 2008, she enrolled for Master‘s Program in Electrical Engineering at the University of Kentucky in Fall 2008. She, during her Master‘s program, worked as a researcher in the field of nanotechnology and developed carbon nanotube sensors for gas detection.